THESIS

A COMPARISON OF AIR SAMPLES AT GROUND LEVEL AND AERIAL GAMMA COUNT RATES FROM THE RESPONSE TO THE FUKUSHIMA DAI-ICHI NUCLEAR POWER PLANT ACCIDENT

Submitted by

Sarah Miriam Sublett

Department of Environmental and Radiological Health Sciences

In partial fulfillment of the requirements

For the Degree of Master of Science

Colorado State University

Fort Collins, Colorado

Summer 2014

Master's Committee:

Advisor: Alexander Brandl

Sandra Biedron
Thomas Johnson

ABSTRACT

A COMPARISON OF AIR SAMPLES AT GROUND LEVEL AND AERIAL GAMMA COUNT RATES FROM THE RESPONSE TO THE FUKUSHIMA DAI-ICHI NUCLEAR POWER PLANT ACCIDENT

March 11, 2011 will be a day that will never be forgotten in the minds of the thousands of Japanese people whose lives were forever changed by a series of natural disasters, including a 9.0 earthquake and subsequent tsunami that triggered the Fukushima Dai-Ichi Nuclear Power Plant (FDNPP), located on the eastern coast of Japan, to become cripplingly damaged. The FDNPP nuclear accident resulted in the emission of radionuclides into the environment and those released nuclides, specifically ^{134}Cs, ^{137}Cs, and ^{131}I and their measurement by ground and air based means, are the subject of this research project. Within the first few days following the start of the disaster, numerous US federal agencies responded and deployed to Japan to help characterize and measure the release of radionuclides from FDNPP. Over the course of approximately a two-month span, over 500,000 measurements were obtained and analyzed, including air and soil samples and in situ spectra. The core of this research project was to analyze and compare ground air samples to aerial gamma count rate measurements obtained in Fukushima Prefecture within the first two months following the disaster. The results of this project estimate the ground deposition of radionuclides in Fukushima Prefecture, which accounted for 99.4% of the measured aerial net gamma count rate. Another finding of this project is the estimated ground deposition of nuclides based upon aerial gamma count rates in areas where there was measurable ground air contamination was 14.25 times higher than in areas where there was no measurable ground air contamination as determined by the evaluated air samples in this project. Of the samples evaluated in this project, ground deposition averaged 5.4E6 Bq/m^2 in areas where there was measurable ground air contamination, versus 3.79E5 Bq/m^2 in areas where there was no measurable ground air contamination.

ACKNOWLEDGEMENTS

I would like to express my gratitude to my advisor, Dr. Alex Brandl, for all of the help and encouragement throughout my time as a student at Colorado State University. I would also like to thank the team of scientists at the Remote Sensing Laboratory at Nellis Air Force Base, Las Vegas, NV for providing access to their valuable data and expertise, without this, I would not have had a project.

I would also like to acknowledge the Health Physics class of 2014 for all of their help and camaraderie; these last two years would not have as much fun or rewarding without all of you.

I would be remiss if I did not express my utmost gratitude to my amazing husband, Reuben, for without his support, none of my accomplishments would ever be possible.

TABLE OF CONTENTS

INTRODUCTION

Fukushima accident:

The Great East Japan earthquake shook the northeastern coast of Japan with an intensity of 9.0 on the Richter scale on 11 March 2011 at 2:46 pm. (Fujiwara, et al., 2012) The earthquake triggered massive tsunamis displacing seawater over 560 km^2 of dry land, the damage from these two events resulted in over 19,000 lives lost and over a million buildings being partially collapsed or destroyed. (World Nuclear Association, 2014) This devastating series of events was further complicated by the fact that 14 nuclear power reactors at four nuclear power plant installations (NPP) were located in the path of the devastating earthquake and ensuing tsunami. Of the 14 nuclear power reactors, 11 were in service at the time of the earthquake, the three non-operational ones were receiving regular maintenance. (Baba, 2013) As part of the standard operating procedure of a nuclear power plant, once the earthquake was sensed, all of the reactors shut down automatically and began cooling their reactors. Six of the nuclear power reactors in the path of the devastation were at the Fukushima Dai-Ichi NPP (FDNPP) operated by Tokyo Electric Power Company (TEPCO). They were boiling water reactors (BWRs) brought into operation between 1971 and 1979, protected by a 10 m sea wall. (Steinhauser, Brandl, & Johnson, 2014) When fully operational, FDNPP provided a total of 4.7 gigawatts of electrical power, making it one of the 15 largest nuclear power installations in the world. (Thakur, Ballard, & Nelson, 2013) FDNPP was equipped with 13 emergency power generators; unfortunately 12 out of the 13 generators became inoperable when seawater from the 14-meter high tsunami engulfed the coastal NPP. (Fujiwara, et al., 2012)

Several events associated with the damaged FDNPP resulted in release of radioactive materials into the environment, including planned and unplanned venting of the reactor vessels, leakage of highly contaminated water from containment, associated fires, and possible partial core meltdowns. Atmospheric releases began on 12 March 2011, with the greatest release phase from 14-17 March, and additional events on 21-23 March, causing widespread contamination of agricultural lands, woodlands, and urban areas of eastern Japan. (Thakur, Ballard, & Nelson, 2013) (Terada, Katata, Chino, & Nagai, 2012) From the initial characterization of the FDNPP accident; there have been numerous estimations as to the source term of released radioactivity.

"The radioactivity released was dominated by volatile fission products including isotopes of the noble gases xenon (^{133}Xe) and krypton (^{85}Kr), iodine (^{131}I, ^{132}I), cesium (^{134}Cs, ^{136}Cs, ^{137}Cs), and tellurium (^{132}Te)" (Thakur, Ballard, & Nelson, 2013). The total amount of radionuclides released into the atmosphere between 12-31 March 2011 is estimated to be approximately 1,020 PBq, after this time frame, only very small amounts were released into the atmosphere. (World Nuclear Association, 2014) Based upon TEPCO's published estimates in May 2012, FDNPP "released a total of about 500 PBq of ^{131}I, 10 PBq of ^{137}Cs, and 10 PBq ^{134}Cs into the atmosphere" from 12 March to 31 March 2011, with approximately 500 PBq of noble gases, primarily ^{133}Xe. Of the entire released radioactivity, around 20% came from Unit 1, 40% from Unit 2, and 40% from Unit 3. (Thakur, Ballard, & Nelson, 2013)

The damage caused by the earthquake, tsunami, and ensuing radiological accident prompted the evacuation of over 300,000 people from Fukushima Prefecture; many still remain evacuated from their homes three years following the disaster. (Smith, 2013) Residents living inside a 20 km radius from the FDNPP and those residing in highly contaminated areas outside this perimeter were evacuated due to the radiation hazard presented by the FDNPP. (Fujiwara, et al., 2012)

Due to the high level of radioactive materials released in the first few days following the accident, Fukushima was rated a level 7 event, the highest level event and the same level also given to Chernobyl, on the International Nuclear Event Scale (INES). While the release from the FDNPP accident was significant, the levels are not considered a public health concern. This in large part is due to the fact the releases occurred when favorable weather patterns transported the majority of the radionuclides into the atmosphere and away from land over the Pacific Ocean. It should be noted that Fukushima radionuclides were detectable as far away as China and the Philippines; very little deposition of radionuclides from the accident was received in countries outside of Japan. (Thakur, Ballard, & Nelson, 2013)

Comparing Fukushima to Chernobyl:

The impact of the FDNPP accident is best understood by comparing it to another well-known nuclear power plant accident, specifically the 26 April 1986 nuclear power plant meltdown at Chernobyl. Both

Fukushima and Chernobyl have been classified as level 7 accidents, the highest on the scale, but there are key differences in their causes and impacts.

The Chernobyl NPP accident occurred as a direct result of inappropriate operator actions during the course of an experiment on Unit 4, involving the RBMK-1000 graphite moderated, light water-cooled reactor operating at low power level. The operation of the reactor outside its safe limits led to xenon-poisoning of the reactor, which was not properly recognized by the operators, who reacted by improper operation of the reactor's control rods, leading to thermal destruction of the reactor by sudden power excursion, resulting steam explosion, and subsequent ignition of the graphite moderators. The reactor was designed without a full containment vessel, allowing the release of a large amount of radionuclides from the reactor into the environment, which continued over a 10-day period following the initial explosion while the graphite moderators burned. (Steinhauser, Brandl, & Johnson, 2014) FDNPP reactors were designed with full containment, which allowed for the controlled release of radionuclides in order to relieve the pressure within the system. The releases from Chernobyl were continuous and uncontrolled, unlike with Fukushima, where the releases were controlled and targeted to ensure that the releases of radionuclides into the environment were performed is such a manner as to allow the least amount of radioactive contaminant into the surrounding area. It is estimated that 80% of the release from Fukushima occurred when favorable winds pushed the plume out to the ocean and away from land. (Steinhauser, Brandl, & Johnson, 2014) While both accidents at Chernobyl and Fukushima resulted in radionuclide contamination and are categorized as level 7 accidents, the impact from Fukushima is far less than that of Chernobyl. Table 1 details some of the main differences in the two accidents.

Table 1: Comparison between Chernobyl and Fukushima accidents (Kortov & Ustyantsev, 2013) (Steinhauser, Brandl, & Johnson, 2014)

	Chernobyl Accident	**Fukushima Accident**
Amount of activity released into atmosphere	5.3×10^{18} Bq	5.2×10^{17} Bq
Area contaminated within country	450,000 km^2	8,000 km^2
Area contaminated other countries	250,000 km^2 in Western Europe	None
Area evacuated	10,800 km^2	1,100 km^2
Population evacuated due to radiation	400,000	83,000
Lives lost from Acute Radiation Syndrome	28 (within 4 months of accident)	0

By comparing the source term of both accidents alone, Chernobyl released 5300 PBq, which is about 10 times more than Fukushima, which released about 520 PBq, excluding noble gases for both accidents. (Steinhauser, Brandl, & Johnson, 2014) Environmental impact monitoring following both accidents reveals that Chernobyl had a much greater effect than Fukushima, which is demonstrated by the smaller highly contaminated areas and the evacuation areas of Fukushima when compared to those for Chernobyl. Additionally, the projected health effects in Japan are significantly lower than after the Chernobyl accident. This is mainly due to the fact that food safety campaigns and evacuations worked quickly and efficiently after the Fukushima accident. In contrast to Chernobyl, no fatalities due to acute radiation effects occurred in Fukushima. The releases within a 30 km radius of the failed Chernobyl reactor were so intense that they caused grave health consequences for the liquidators as well as causing a "nuclear sunburn" from beta radiation on the exposed hands and faces of the first liquidators as well as "nuclear quinsy," described as a continuous hoarse cough caused by burns to the throat and bronchia. (Kortov & Ustyantsev, 2013) No such effects have been reported from Fukushima.

What is gamma spectrometry?

In order to properly characterize the released radionuclides and subsequent impact following a radiological event such as Fukushima, the use of gamma spectrometry is a necessary and important tool. While Fukushima released nuclides with alpha, beta, and gamma radiation, detection of gamma radiation and determining the radionuclide from which it was emitted is simpler, quicker, and better fit for this type of environment. Gamma spectrometry is the evaluation of the energy signals or spectra from ionizing radiation and the determination of the associated nuclide responsible for emitting the gamma ray detected.

A gamma ray photon travels a much further distance than alpha or beta radiation, allowing it to be detected from a much greater distance than the other two. Gamma ray photons are uncharged and produce no direct ionization or excitation of the material they pass through. Gamma ray detection is heavily reliant on the gamma ray photon interacting with the absorbing material within the detector and transferring all or part of its energy to an electron. Without this transfer and creation of a photoelectron, the detector has no way of seeing or characterizing the incident gamma ray. The maximum energy of these electrons equals the energy of

the incident gamma ray minus the electron binding energy. The electron will lose its energy through ionization and excitation of atoms within the absorbing material and through bremsstrahlung emission. A gamma ray spectrometer must function as a conversion medium with a reasonable likelihood of interaction with incident gamma rays yielding at least one electron and it must also be capable of detecting the secondary electrons produced. (Knoll, 2010)

In-situ gamma spectroscopy was introduced in 1972 "to determine the concentration of natural and artificial radionuclides in soil, the relevant outdoor gamma dose rate in the air above, and the relative contribution of the U-238 and Th-232 series and K-40 to the dose rate" (Nuccetelli, 2008). In-situ gamma spectroscopy originally employed two basic assumptions: the source must be capable of being modeled as an infinite half-space and the vertical distribution of radionuclides is uniformly distributed for natural radionuclides and exponentially distributed for artificial radionuclides. (Nuccetelli, 2008) Continuing research in the field rendered these assumptions unnecessary and in-situ gamma spectrometry is now independent of source geometry and vertical distribution of the radionuclides, as well as making this technique applicable in indoor scenarios. (Nuccetelli, 2008) By providing "rapid and integrated measurements of the investigated environment and dose rate contributions of radionuclides" (Nuccetelli, 2008), in-situ gamma spectroscopy has become a powerful tool for environmental monitoring in numerous research, routine, and emergency applications. For example, in-situ gamma spectroscopy has been used to characterize sites in terms of natural background radiation, characterization of contamination by NORM and/or artificial radionuclides, measurement of nuclear weapons fallout, accidental releases from nuclear power plants as well as radionuclide characterization following a nuclear power plant accident, like Fukushima.

In-situ gamma spectrometry "provides not only qualitative information (identification of radionuclides by the corresponding peak positions) but also quantitative information (photon flux energy distribution at the point of measurement)" (Kluson, 2010). Quantitative information is not generally available immediately since the spectra need to be processed and the efficiency of the detector based upon the radionuclides seen needs to be established before this information is known.

Aerial in-situ gamma spectrometry or airborne gamma spectrometry (AGS) works by averaging values from relatively large areas, given as a function of the aircraft's altitude and speed and the acquisition time of one spectrum. (Kluson, 2010) Factors that also contribute to the footprint are the gamma ray energy and the atmospheric attenuation of the gamma rays, allowing the detector array the capability of detecting gamma rays from large distances. The atmospheric attenuation shields the distant gamma rays from detection, making the gross gamma count rate more of an average count rate, than a precise one. (Lyons & Colton, 2012) Figure 1 depicts the orientation of aerial in-situ gamma spectrometry with respect to aircraft altitude. The ground surface area or detector field of view (FOV) represented by a given spectrum is generally accepted to be a circle with a radius equal to the above ground altitude of the aircraft. (Lyons & Colton, 2012)

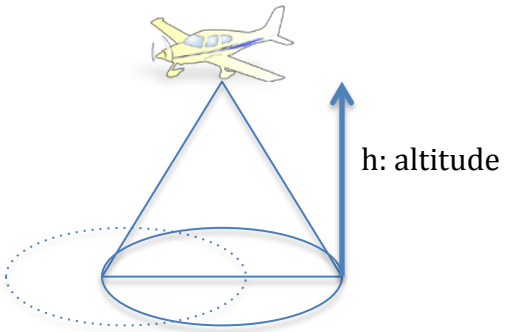

Figure 1: Airborne gamma spectrometry (AGS) orientation.

AGS is an essential tool for prompt and wide-ranging nuclide specific characterization of contamination following an accidental release of radionuclides from a nuclear facility, geological mapping, determination of cause of irregularities of natural radionuclides, assessment of uranium mine site rehabilitation, mineral exploration, and detection of lost radioactive sources. (Kock & Samuelsson, 2011) The low flying aircraft used in AGS typically operates with 30 - 100 m ground clearance and is capable of mapping the gamma ray emitting radiation distribution at ground level at a rate 10^2 – 10^3 times faster and covering areas 10^6 – 10^7 times greater than other ground-based methods. (Sanderson, Cresswell, Hardeman, & Debauche, 2004) The aircraft used in this application of gamma spectrometry are usually equipped with a large-volume sodium iodide (NaI(Tl)) detector array coupled with a high purity germanium-semiconductor (HPGe) detector. The HPGe-detector more clearly identifies individual radionuclides than the NaI(Tl)-

detector, but takes longer to determine the results. (Winkelmann, Strobl, & Thomas, 2004). The advantages of using a NaI(Tl)-detector when compared to other detectors, like the HPGe, is that it requires less time, its highly portable and less expensive. (Caciolli, et al., 2012). Some of the parameters affecting the gamma radiation field when using AGS are the topography, soil density, moisture, and geology. (Kock & Samuelsson, 2011) Kock and Samuelsson conducted a study where they compared airborne and terrestrial gamma spectrometry measurements and found that "the spatial correlation between AGS and ground data is stronger in areas where the activity variability is large; given a large enough mean activity" (Kock & Samuelsson, 2011).

When conducting a routine or non-emergency survey of a small area, ground-based mobile in-situ gamma spectrometry is seen as a good alternative or compliment to AGS. The advantage of using the ground-based method is that there is better spatial resolution. However, the difference in the field of view for a ground based mobile in-situ gamma spectrometry versus an aerial one makes the comparison between the two less straight forward. (Kock & Samuelsson, 2011). During each AGS flight, "sequences of gamma ray spectra, geographic positioning information and ground clearance data are recorded, and are used to quantify levels of individual radionuclides and the general gamma-dose rate. This results in a practical means of conducting surveys with total effective coverage" (Sanderson, Cresswell, Hardeman, & Debauche, 2004). The information gained from an AGS flight can then be used to find a missing source, plot a plume, or characterize the background radiation for the surveyed area.

There are many successful examples where AGS has been used to identify and locate missing sources, including "the urban area of Goiania in Brazil, following the dispersion of Cs-137 in the form of CsCl salt when a hospital radiotherapy unit was dismantled" (Cresswell & Sanderson, 2012). AGS not only proves useful in finding sources, but also is capable of demonstrating the "absence of sources > 5-10 MBq Cs-137 within large areas, and identify areas where patchy anthropogenic distributions would require further ground based investigations to confirm the absence of sources. Rates of area coverage and detection for relevant sources significantly in excess of ground based approaches have been demonstrated" (Cresswell & Sanderson, 2012). One of the main advantages of AGS is that it can help focus ground based efforts and remediation, which can be very time consuming and expensive.

Air sampling:

An air sampling system is composed of three main components, all requiring proper calibration: a vacuum pump to draw air through the system, a collection device to separate the contaminant from the air, and a metering device to measure the volume of air sampled. (Cember & Johnson, 2009) The airborne radioactivity concentration is determined by dividing the quantity of activity collected by the sampled air volume. The most common type of collection device is filtration. There are several types of collection devices or sampling media including glass fiber, paper, and membrane; the type used depends on the characteristics of the target contaminant or the goal of the measurement. (Cember & Johnson, 2009) When sampling for iodine, air is pulled through a cartridge containing activated charcoal which binds to the iodine. With all air samples, the collection device or sampling medium requires further analysis, generally in a lab, to determine the captured contaminant. A hasty measurement can be made at the time of the filter exchange, but generally, it is best to evaluate each sample in the lab where more robust detectors are available.

Response to Fukushima:

As soon as the gravity of the events on 11 March 2011 were felt across the globe, many scientists and response teams, with their home nation's reach-back capabilities, flocked to Japan to help with humanitarian relief, disaster assessment, area stabilization, and recovery efforts. (VanHorne-Sealy, Livingston, & Al, 2012) With numerous US military personnel and their families residing in Japan, the US had a vested interest in ensuring the safety of Americans, as well as a duty to help out an ally during a tragic event. "The US government maintains the capability to respond to real or perceived release of radiological or nuclear material into the environment" (Blumenthal, Bowman, & Remick, 2012). The US responded by activating the US Department of Energy's Nuclear Incident Team (NIT) on 11 March 2011 to act as a command center coordinating all US efforts in Japan. The NIT coordinated the following agencies: "US Department of Energy National Nuclear Security Administration (DOE/NNSA) Consequent Management (CM) assets, which include the Aerial Measuring System (AMS), the National Atmospheric Release Advisory Center (NARAC), the Consequence Management Response Team (CMRT), the Consequence Management Home Team (CMHT), and the Radiation Emergency Assistance Center/Training Site (REAC/TS)" (Blumenthal,

Bowman, & Remick, 2012). The NIT remained operational in Japan until 28 May 2011, when all activated US assets returned. DOE/ NNSA's Radiological Assistance Program (RAP) and Radiological Triage program also provided additional assistance. During an incident in the US, the Federal Radiological Monitoring and Assessment Center (FRMAC) coordinates all federal agencies responding to a radiological incident. FRMAC is responsible for the "collection, analysis, and assessment of environmental radiological data" (Blumenthal, Bowman, & Remick, 2012) and coordinating the release of products to the decision makers. Although the incident was not on US soil, FRMAC played its role by coordinating the efforts of those agencies responding to Fukushima and has been the repository of radiological data analyzed and collected from Fukushima.

The NIT first activated NARAC, who provided initial atmospheric plume predictions without any radiation source term data to provide the emergency manager with enough information to make the decision as to whether to direct protective action and if so, at what level. As time progressed and more data were collected, NARAC updated their plume predictions and the emergency manager to make more informed decisions and directives as well as providing guidance to the US in the event of any necessary actions to be taken on US soil as a result of their predictions.

Due to the nature of their responsibilities, NARAC was able to begin working immediately, but it took the DOE/NNSA a few days to arrive on scene in Japan and begin operations there. Once in country, the DOE/NNSA's AMS were able to begin initial data collection using their tested AGS systems on aircraft already in country within 12 hours and proceeded to log over 500 flight hours over the course of the two-month span of their deployment. (Blumenthal, Bowman, & Remick, 2012) AMS was able to provide the data necessary to validate and enhance the plume models produced by NARAC. Ground measurements which included air and soil samples, contamination swipes, exposure rates, and in-situ gamma spectroscopy, were also obtained and used to calibrate and normalize the AGS measurements. (Blumenthal, Bowman, & Remick, 2012) The teams deployed to Japan were limited in personnel, but had extensive reach back capabilities which included a large number of scientist and support staff with a large variety of specialties, including nuclear physics, health physics, geographic information systems, analysts, and logistical support staff. (Blumenthal, Bowman, & Remick, 2012) Over the two-month span of time, a substantial amount of data was collected and

analyzed. The main objectives of data analysis included "defining the mix of radionuclides released from the reactor, characterizing the inhalation component of integrated dose, and assessing the vertical and horizontal migration of deposited material in the soil." (Blumenthal, Bowman, & Remick, 2012). Once the data were analyzed, they were used to produce maps that were then used by the decision makers, including the US Military, the US Department of State, the White House, and the Japanese Government, to define "relocation zones, inform decisions on agricultural products, determine stay times for responder safety, identify safe transportation corridors, and for many other purposes," (Blumenthal, Bowman, & Remick, 2012), as well as planning humanitarian activities, risk evaluations, travel advisories, and protective measures for the population and responders. The importance and validity of the data were crucial because it could impact tens of thousands of people, so all data were very closely monitored and checked when making the maps.

Responder safety was also taken very seriously, which is shown by the fact that "despite traveling to within several kilometers of the Fukushima Daiichi Nuclear Power Plant or flying aerial radiological survey missions when airborne releases were still occurring, none of the 100 DOE/NNSA responders who spent time in Japan received any recordable radiation dose (i.e., each was < 0.15 mSv total dose)" (Blumenthal, Bowman, & Remick, 2012). This is a testament to not only individual safety and precautions taken, but also the skilled level to which the responders were trained.

AMS background and response to Fukushima:

The DOE/NNSA's AMS is a response asset initially established to support the aboveground nuclear testing program in the 1960's at the Nevada Test site. AMS is designed to respond quickly to a radiological emergency event and utilizes dedicated fixed and rotary winged aircraft along with advanced radiation detection systems. AMS maintains two bases of operation within the US, one at Nellis Air Force Base in Las Vegas, NV and the other at Joint Base Andrews Naval Air Facility located just outside of Washington, DC. (Lyons & Colton, 2012) The mission of the AMS "is to provide a rapid and comprehensive worldwide aerial measurement, analysis, and interpretation capability in response to a nuclear/radiological emergency" (Lyons & Colton, 2012).

The fixed-wing aircraft is designed to produce a ground deposition map with a one-meter above ground exposure rate equivalent, used to amend or authenticate the deposition models produced by NARAC. The ground deposition map produced by the fixed-wing data analysis does not generally account for cosmic radiation, radon, natural terrestrial background radiation, or aircraft background, making its work product coarse, but sufficient for comparison, given its mission requirements. (Lyons & Colton, 2012)

AMS uses a detector pod containing three 5 cm × 10 cm × 40 cm (2" × 4" × 16") NaI(Tl) crystals with two to three pods per aircraft, depending upon availability of units and mission requirements. During their response to the Fukushima accident, AMS deployed with a total of four Radiation Solutions Inc. (RSI) RSX3 detector pods (Lyons & Colton, 2012).

AMS aircraft ground speed, line spacing, and altitude are set based upon optimization of the detector system's spatial resolution and sensitivity given the existing survey data and the current NARAC deposition model, as well as ensuring a safe flight configuration and time constraints. AMS uses two different types of aircraft to obtain their data, one is a fixed wing aircraft and the other is a rotary wing aircraft. Fixed-wing aircraft conducting a survey over populated areas generally travel at a speed of 140 knots with an altitude of 1000 ft and flight line spacing of 2000 ft. Rotary-wing aircraft conducting a survey over populated areas generally travel at a speed of 70 knots, with an altitude of 500 ft and flight line spacing of 1000 ft. (Lyons & Colton, 2012) The advantage of a fixed-wing is that it can carry more weight and equipment than a rotary-wing aircraft, but it cannot fly as low as a rotary-wing aircraft.

AMS's response to the Fukushima accident spanned 14 March – 28 May 2011, where they collected data over the course of 100 survey flights spanning 525 flight hours, all planned to avoid any encounters with an airborne plume. (Lyons & Colton, 2012) During the response to Fukushima, "aerial data includes gamma count rates and 1,024 channel spectra acquired at 1-s intervals correlated with GPS latitude/longitude coordinates. The gamma count rates acquired at survey altitude are extrapolated to one meter above ground using air attenuation coefficients and then converted to 1-m exposure rates" (Lyons & Colton, 2012). The nature of the response to Fukushima was unique in that there was airborne radioactivity present, but the normal geometry of the systems could not distinguish between airborne and ground deposited radioactivity.

Several different configurations were tested during the beginning of the response to determine the best geometry to enable AMS to discern between airborne and ground based radioactivity, ultimately placing the detector in the aircraft in an area that was not shielded by aircraft components proved to be optimal. (Lyons & Colton, 2012)

AMS conducted two different types of calibration flight lines, the test line and the water line. The test line, flown at the beginning and end of each flight, was to verify the stability of the system and determine if the background radiation level changed during the course of the flight. The test line is flown at the altitude and speed of the survey over a relatively short (two to three kilometers), easily recognizable flight path, void of any artificial radioactive contamination with a relatively constant count rate. There is generally variation between test lines from one flight to the next, based on changes in radon or airborne contamination, but adjustment for these variations is performed to match the survey data from one flight to the next. (Lyons & Colton, 2012) The water line is also flown at survey altitude and speed over a sufficiently large body of water whose detector field of view excludes the shoreline for at least a minute and is used to determine the background radiation count rate when there is no terrestrial radiation present. (Lyons & Colton, 2012) The water line will contain count rate contributions, which consist of cosmic rays, airborne contamination, aircraft and equipment contributions, as well as gamma rays from radon and its airborne progeny. (Lyons & Colton, 2012)

Ground air sampling:

The majority of the contamination released from FDNPP was airborne, so one of the important survey techniques used to quantify and characterize airborne contamination was ground air sampling. "Representative measurements require ideal operating conditions, e.g. unhindered air flow from all directions and 100% aerosol collection efficiency. In most cases, however, these conditions are not given in reality" (Wershofen, 2013). The specific air sampling systems and media used to sample the ambient air in Fukushima prefecture and other areas of interest in response to the FDNPP accident were the DF-AB-40L Emergency Response Sampling System, coupled with Hi-Q model FP2063-20 glass fiber filters for particulate collection and Hi-Q TC-12 TEDA impregnated carbon cartridges for collection of iodine. (Mena, Pemberston, & Beal,

2012) Ten-minute grab samples were taken for routine field measurements. No specific information regarding the exact conditions or specific collection efficiency are known, but it is important to note that "a range of variability of up to ±40% can be applied for the radionuclides which occur in smaller activity concentrations" (Wershofen, 2013).

Nuclide ratios:

Understanding the radionuclides released from FDNPP and their characteristics and activity ratios was important in determining how to allocate assets in response to the accident, as well as how, when, or if any protective measures need to be put into place. The main nuclides of concern following FDNPP were ^{131}I, ^{134}Cs, and ^{137}Cs. ^{131}I occurs most readily as a vapor, whereas cesium has a high affinity to bond to aerosols and is subject to both wet and dry deposition. The ratio between ^{134}Cs and ^{137}Cs can be used to distinguish between nuclear weapons testing fallout and the release of fission products from a NPP, due to their different half-lives. The $^{134}Cs/^{137}Cs$ ratio can also be used to separate samples from Chernobyl and Fukushima. The average $^{134}Cs/^{137}Cs$ ratio from Fukushima is calculated to be around 1, but samples obtained from Fukushima prefecture and surrounding areas have been found to be 0.8 – 0.9. (Thakur, Ballard, & Nelson, 2013) The significance of a $^{134}Cs/^{137}Cs$ ratio of 1 is that it is suggestive of a release from a nuclear reactor, not nuclear weapons testing. Another telling finding is the presence of ^{132}Te, which is mainly released from active fuel rods, not spent nuclear fuel. (Thakur, Ballard, & Nelson, 2013) The $^{131}I/^{137}Cs$ activity ratio may indicate the age of the nuclide mixture and transport time from its source, due to ^{131}I's relatively short half-life of 8 days, compared to that of ^{137}Cs with a half-life of the approximately 30 years. During 14 March - 5 April 2011, the activity ratio of measured particulate $^{131}I/^{137}Cs$ ranged from 1.1 to 131, with the peak values observed 15 - 17 March and 21 - 24 March. (Thakur, Ballard, & Nelson, 2013).

Impact of environment and nuclides released following the Fukushima accident:

"Climatic, geographic, ecosystem, living and dietary habit differences, as well as economic and social conditions, can affect the transfer of radionuclides through the food chain and the doses to human populations" (Tracy, et al., 2013). Radioecological sensitivity is the analysis of the combinations of those

factors, which contribute to the highest doses, and understanding of the factors is vital for scientists and decision makers to effectively mitigate and manage the risks associated. (Tracy, et al., 2013)

"From a radiological point of view, ^{131}I and ^{137}Cs are the most important radionuclides to consider, because they are responsible for most of the radiation exposure received by the general population" (Thakur, Ballard, & Nelson, 2013). Given identical releases modeled following a major nuclear accident, the highest predicted doses resulted from the ground deposition of ^{137}Cs across agricultural, forest or tundra, coastal marine, and freshwater aquatic environments, when compared to ^{90}Sr and ^{131}I. (Tracy, et al., 2013) The highest dose to an adult from ^{137}Cs deposition was found to be in an agricultural environment, then in a forest setting, then lake and lastly marine. ^{131}I becomes a greater hazard in the marine environment due to the "enhanced uptake by seaweeds," (Tracy, et al., 2013), given the high consumption of seaweed in the Japanese culture, this is also of concern. "The two factors that had the greatest influence on the variability of radiation doses were the time of year when the deposition occurred and the consumption rates of contaminated food items" (Tracy, et al., 2013). This difference could account for as much as two orders of magnitude of predicted dose, depending on whether the deposition occurred during the peak growing season, or after all crops were harvested, making the impact of the Fukushima accident lower due to the fact it occurred prior to the start of the agricultural season. (Tracy, et al., 2013) "Releases of radio-iodine from a real nuclear event are expected to be considerably higher than those of radiocesium, due to the higher volatility of iodine. UNSEAR (2008) indicates that ^{131}I releases from Chernobyl were of the order of 1800 PBq, 20 times as high as the estimate of 86 PBq for ^{137}Cs" (Tracy, et al., 2013).

MATERIALS AND METHODS

Compiling the data:

The data used in this work came from two main sources, both under the Department of Energy's (DOE) National Nuclear Security Administration (NNSA): aerial gross gamma count rate data from the Remote Sensing Laboratory (RSL)'s AMS and lab-processed ground-based air samples from the Federal Radiological Monitoring and Assessment Center (FRMAC). Both data sets are massive and required extensive paring down to obtain a manageable, yet still descriptive and large data set to be further evaluated. The timeframe represented by the RSL data included aerial measurements from 15 March 2011 through 10 May 2011, which included over 100 aerial flights and over 525 hours of flight time. The set of ground-based air samples obtained from FRMAC's database include those samples obtained from 13 March - 10 May 2011. The measurements contained in both data sets were tagged with Global Positioning Satellite (GPS) coordinates, allowing for the comparison of the measurements. The GPS coordinates provided with the samples varied in length between four and seven decimal places; for consistency of measurements and evaluation, all given GPS coordinates were rounded to five decimal places to be within one meter from the exact location. (Bartlett, 2007) "Over 500,000 fixed and handheld instrument-derived exposure/dose rate measurements, data from over 500 different flights, more than 600 air sample media pairs, 89 soil cores, and hundreds of in situ spectra all collected/transcribed by roughly 200 responders, there were some issues with incomplete data" (Mena, Pemberston, & Beal, 2012). Efforts have been made to fill in any gaps in data.

Characterization of data sets:

The two data sets compared during this project are ground based air samples and aerial gross gamma count rate measurements. The ground based air samples represent activity concentrations, reported in units of μCi/mL, which represents the concentration of radioactive material present in the air sampled, but does not include any ground deposition or an exposure rate and is directly tied to the specific nuclide(s) detected in each sample. The aerial gross gamma count rate measured and reported by AMS survey flights is reported as counts per second (cps), representing the total activity over the given area, is independent of any information on the origin of the radiation, as far as its location (ground deposition or air) or any specific nuclide

information. In order to provide a comparison of the two different data sets and provide meaningful results, further analysis of the data and systems used to obtain the data was required.

The three nuclides of interest for this project were ^{131}I, ^{134}Cs, and ^{137}Cs. These three nuclides were selected based upon being gamma emitters, their individual half-lives, and their association with a release following a nuclear power plant accident. Table 2 depicts the pertinent information for these three nuclides that were used for this project.

Table 2: Half-life, gamma constant, and summed branching ratios for the three nuclides of interest for this study. (Johnson & Birky, 2012)

Nuclide	Half-life	Gamma Constant (Gy-m² per Bq-s)	Summed Branching Ratio
^{134}Cs	2.0648 y	5.79E-17	0.918
^{137}Cs	30.07 y	2.27E-17*	0.851
^{131}I	8.0207 d	1.45E-17	0.790

* Note that the gamma constant used for ^{137}Cs is that of ^{137m}Ba

Assumptions made during data analysis:

Some of the data were difficult to interpret and required additional assumptions in order to fill in the gaps where information was either incomplete, or necessary in order to effectively compare the given data. The results of the ground air samples are considered to include the efficiency of the air sampling systems and lab detectors. Ground air sample results are assumed to be representative of the plume or column of air from the location from which the samples were collected. For comparison between the ground air sample data and the AGS data, the activity concentration reported by the ground air sample measurements characterized the activity concentration for the entire column of air for the pair of ground and AGS data points from the ground to the survey flight altitude. These assumptions provide an opportunity for further study and provide insight into the nature of the radiation measured by the aerial survey flights that were not accounted for by the ground air samples.

FRMAC:

FRMAC has a log of approximately 1700 individual ground-based air samples obtained throughout Japan, with the main concentration in and around Fukushima Prefecture following the FDNPP disaster from 13 March 2011-14 January 2012. Just over 800 individual ground air samples taken between 13 March and 10 May 2011 were used for comparison. The FRMAC database contains approximately 10,000 corresponding

results to those 800 individual samples. The large difference between the number of samples and the number of results is based upon the method of evaluation that was performed on the sample and the various nuclides for which it was evaluated, in the case of gamma spectrometry. The nature of the ground measurements were air samples that were obtained on filters and sent to a qualified lab where gamma spectroscopy was conducted on them using counting times ranging from 20 minutes to several days. The contract lab also evaluated the samples using a variety of methods including: alpha spectrometry, liquid scintillation counting (LSC), and Inductively Coupled Plasma-Mass Spectrometry (ICP-MS), but only the samples evaluated using gamma spectroscopy were considered for this project.

Further review of those samples and results narrowed the pool of data to those samples with GPS coordinates geographically within or reasonably close to Fukushima Prefecture that had a result (inclusive of 0 or below Minimum Detectable Activity (MDA)). This further limitation brought the number of samples to 104 and corresponding results down to 312. Note that all samples had results for all three nuclides of interest, albeit some results were 0 or below the MDA. Of those 104 samples, there were 69 different sampling locations evaluated, with 34 locations having two or more samples obtained at that location. For samples obtained at the same locations, generally they had the exact same GPS coordinates or where within a few meters of each other, and some were obtained on the same or different days. Figure 2 is a map of Japan with pins depicting each evaluated ground sample location.

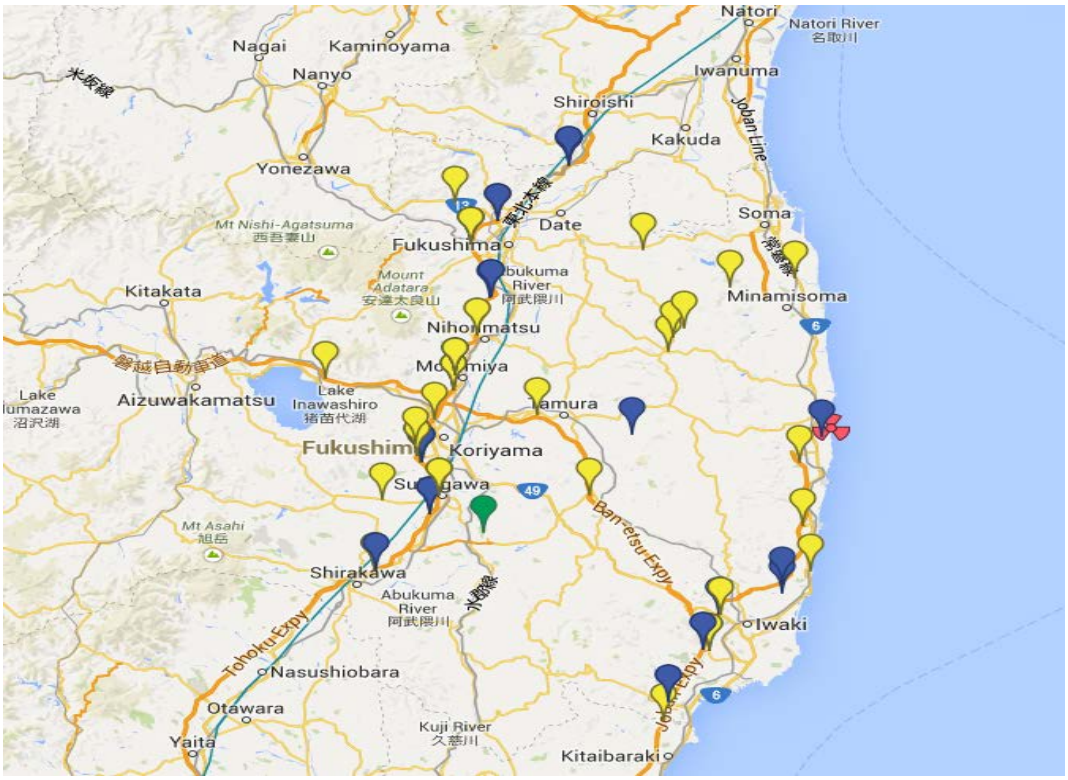

Figure 2: The map depicts the 69 unique locations of the ground-based air samples obtained 13 March through 10 May 2011 and evaluated for use during this project for comparison to the RSL aerial gamma count rate data following the FDNPP accident. The blue pins depict a site where one sample was obtained, the yellow pins depict a site where two samples were obtained, the green pin depicts a site where three samples were obtained, and the red trefoil depicts the location of the FDNPP.

AMS Aerial Data:

The vast amount of data provided by AMS required the use of ArcGIS software, specifically ArcMap to view and mine. Each point of data represents one second of flight time that captures several useable data quantities, including a gamma spectrum and gross gamma count rate, which are all GPS-tagged. Appendix A depicts two different screen shots from ArcMap showing examples of the data available for each data point. While the amount of inputs available for each data point is vast, they require the user to define and link the output to the detectors in order for the information to be useable. For the FDNPP mission, the defined outputs included: identification number, latitude, longitude, altitude above ground in meters, and gross gamma count rate. HPGe spectra were also obtained during the survey flights, but were not geo-referenced, so are not been included with this analysis. AMS personnel reported that for the FDNPP mission, their "key

sources of error were due to the rough, rapidly varying terrain compared to a flat plane for which this procedure is appropriate" (Lyons & Colton, 2012). Every effort was made during data collection and analysis to account for terrain features. The AMS aerial data used for this project were from the manufacturer set parameters, not AMS, which creates an additional level of uncertainty in the data, but that extent is not known to this project team.

Pairing of ground air samples to AMS aerial survey measurements:

All of the AMS aerial flight data and ground air samples within the vicinity of Fukushima Prefecture were uploaded into ArcMap to compare the GPS locations of the ground samples and the aerial survey flight lines. Once entered, a systematic approach was used to evaluate each individual ground air sample location in order to find an aerial measurement that contained the ground sample within its field of view. Numerous ground air samples were obtained outside of the field of view of an aerial measurement, removing the ground air sample from further analysis in the scope of this study. Another factor that removed ground air samples from further analysis was when the coupled aerial survey occurred during a time greater than 10 days either before or after the ground air sample was obtained.

Once analysis of the viability of the ground air samples was completed, a total of 54 different ground air samples, obtained from 36 unique locations, with a total of 112 different results were compared to the aerial measurements. There were 17 ground air samples which measured no detectable activity for any of the three nuclides of interest, but were included in the analysis and comparison of the aerial gamma count data to further evaluate ground deposition. Figure 3 is the revised ground air sample location map with the 36 unique sample locations that were used to compare the aerial gamma count rate data.

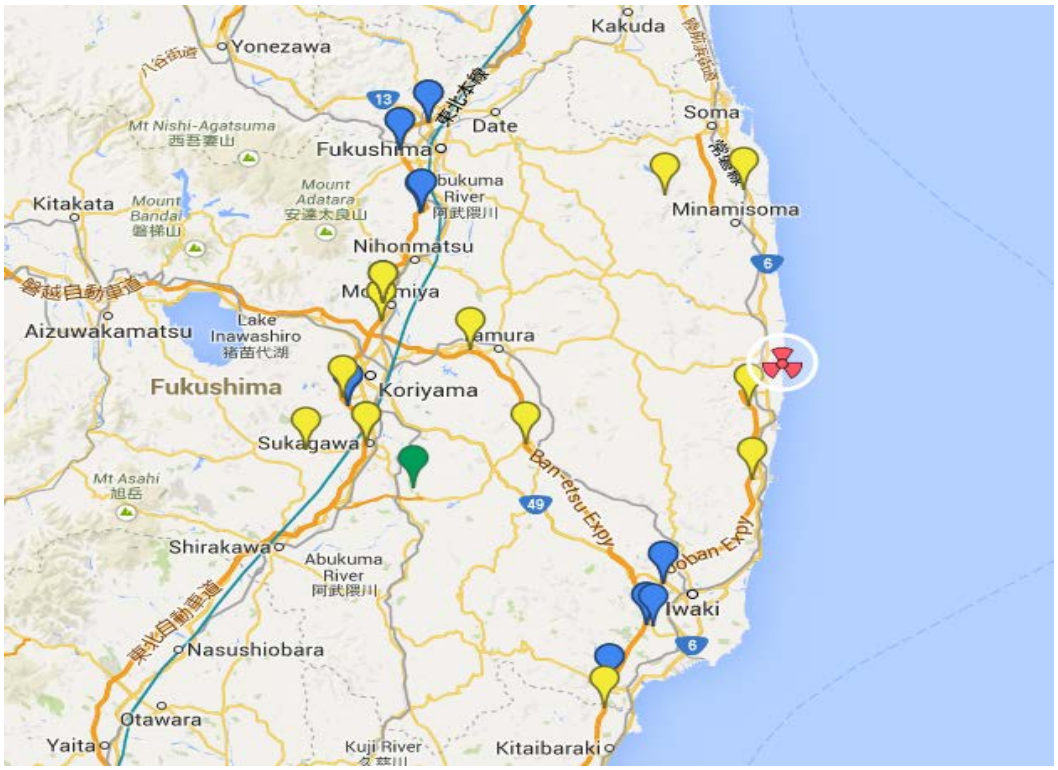

Figure 3: The map depicts the 36 unique sample locations of the ground-based air samples compared to the AMS aerial measurements used during this project. The blue pins depict a site where one sample was obtained, the yellow pins depict a site where two samples were obtained, the green pin depicts a site where three samples were obtained, and the red trefoil depicts the location of the FDNPP.

There were a total of 50 ground air samples removed from analysis for various reasons. Thirty-seven of those ground air samples were removed due to the ground sample lacking an aerial measurement within 10 days of the ground measurement that was within the field of view of an aerial measurement. The 10-day assumption is based upon the decay of the nuclides of interest and variation caused by changes in weather and the airborne contamination being analyzed. The other 13 ground air samples removed from further comparison were due to errors or inconsistencies with the aerial gamma count rate measurements to which they were paired. The original set of ground air samples considered for comparison were collected on 12 different days during the sampling period (March 13, 19-24, 27, April 2, and May 8-10). This pairing down of viable ground air samples to be used also resulted in the majority of the sample collection dates to fall during the time periods of 19-24 March and 8-10 May 2011.

Detector efficiency determined by Monte Carlo N-Particle (MCNP):

Monte Carlo N-Particle (MCNP) is a computer modeling program developed in the 1940's at Los Alamos National Lab during the development of nuclear weapons as a method that uses essentially the game of chance to model large numbers of particle interactions. (Kalos & Whitlock, 2008) The efficiency of the detectors used to obtain the aerial measurements is unknown to the project team, so two different MCNP models were created to simulate the detector's efficiency based on two different source definition scenarios: a plume where the detector is submersed within the source and aerial measurement of ground deposition of the source. Both models were based on determining the efficiency of one detector pod consisting of three 5 cm × 10 cm × 40 cm (2" × 4" × 16") NaI(Tl) scintillation crystals used by AMS to obtain the gross count rate during their response to the FDNPP accident. Only one detector pod was modeled because the limited availability of pods at times during the FDNPP accident response sometimes left a survey flight with only one pod to conduct the measurements. The MCNP model represents a more restrictive estimate of the actual detector efficiency during the response. Note that an F8 tally was used with four energy bins and the total modeled efficiency was calculated by taking the sum of the bins and subtracting those gammas detected that were below 10 keV in energy to more accurately represent the real world scenario being modeled. Lower energy gammas are not measurable by the NaI(Tl) detectors, because below 10 keV is too low an energy to enter into the detector. The other justification for omitting these low energy gammas is that none of the nuclides of interest emit gamma radiation in that energy range and if detected could be from another source of radiation.

To model the submersion or plume scenario for the detector, 500 million particles were sufficient to produce acceptable statistics with uncertainty less than 3%, the input developed for this model is shown in Appendix B. The three nuclides of interest, ^{134}Cs, ^{137}Cs, and ^{131}I were each modeled independently, assuming a homogenous activity concentration within an air space outside of the aircraft housing the detector pod. All three models passed all 10 statistical checks performed by MCNP.

Modeling the efficiency of the detector for the ground deposition required a different model with one billion particles to provide a reasonable estimate with good statistics of the actual efficiency of a single

detector pod. The input file used for this second model is shown in Appendix C. This model required the use of an array of detector pods in order to achieve an acceptable uncertainty averaging 4.29%. Ninety-six different detectors, divided into thirty-two different pods were simultaneously run and their resulting efficiency in particle detected per particle emitted calculated using Equation 1 to obtain the weighted mean efficiency for one individual detector pod. Equation 2 was used to calculate the uncertainty or standard deviation for this result. Multiple models were run; each at different representative altitudes for the aerial survey flights, ranging from 100 m to 550 m in height above ground and a fit parameter was calculated to extrapolate the efficiency of the detector at varying altitudes for each nuclide of interest.

$$\mu = \frac{\sum \frac{x_i}{\sigma_i^2}}{\sum \frac{1}{\sigma_i^2}} = \frac{\frac{x_1}{\sigma_1^2}+\frac{x_2}{\sigma_2^2}+\frac{x_3}{\sigma_3^2}+\cdots}{\frac{1}{\sigma_1^2}+\frac{1}{\sigma_2^2}+\frac{1}{\sigma_3^2}+\cdots} \qquad [1]$$

Where:
$\mu = weighted\ average\ of\ the\ individual\ detector\ efficiencies$
$x_i = efficiency\ of\ detector\ i, in\ particle\ detected\ per\ particle\ emitted$
$\sigma_i = standard\ deviation\ \ of\ detector\ i$

$$\sigma_T^2 = \frac{1}{\sum \frac{1}{\sigma_i^2}} = \frac{1}{\frac{1}{\sigma_1^2}+\frac{1}{\sigma_2^2}+\frac{1}{\sigma_3^2}+\cdots} \qquad [2]$$

Where:
$\sigma_T = standard\ deviation\ of\ the\ weighted\ average\ \mu\ (calculated\ in\ Equation\ 1)$
$\sigma_i = standard\ deviation\ of\ detector\ i$

The associated efficiencies for the three nuclides of interest are given in Table 3 and represent the modeled efficiency of one three-detector pod for a detector submersed within a contamination plume. The associated uncertainties for the efficiency of the detector for all three nuclides were less than 3%.

Table 3: MCNP calculated nuclide efficiencies for a detector submersed within a contamination plume a NaI(Tl) detector pod used by AMS during their response to the FDNPP accident.

Nuclide	Calculated Detector Efficiency for Detector Submersion Scenario (per particle emitted)
^{134}Cs	2.303E-5
^{137}Cs	2.286E-5
^{131}I	2.363E-5

The associated efficiencies for each nuclide at the four different modeled altitudes for a ground deposition source are given in Table 4. The overall uncertainty of the efficiency of the detector for each of the nuclides varied based upon flight altitude, with the least amount of uncertainty being at the lower elevations and the most uncertainty being at the highest elevations. For instance, ^{131}I had the widest range of

uncertainty at different elevations which ranged from 0.5% at 100 m up to 14.6% at 550 m., while both cesium isotopes ranged from 1.6% to 10% for the modeled elevations.

Table 4: MCNP calculated nuclide efficiencies, reported in per particle emitted for each nuclide at each of the modeled altitudes in meters, for a detector pod measuring ground deposition for the NaI(Tl) detectors used by AMS during their response to the FDNPP accident.

	Detector Efficiency for Ground Deposition (per particle emitted) at given Altitude (m)			
Nuclide	100 m	200 m	350 m	550 m
^{134}Cs	3.28E-02	2.35E-02	1.19E-02	5.35E-03
^{137}Cs	2.96E-02	2.19E-02	1.12E-02	3.98E-03
^{131}I	2.55E-02	1.69E-02	6.84E-03	3.16E-03

Determining Background:

The method employed by AMS to determine background radiation for a given geographical area was to establish test lines over geographically similar areas, known or suspected to be free of unnecessary contamination, and to subtract those measurements from the gross gamma count rate obtained during a survey flight over the area of interest. An average background count rate was obtained from a random sampling of eleven different measurements from several representative test line surveys and was used to calculate a net gamma count rate from the gross gamma count rate measurements used to compare the ground air samples to the aerial gross gamma count rates.

Method of data analysis:

All air sample activity concentrations were decay-corrected to the day, at which the aerial survey flight that most closely matched in proximity and time was obtained, and based on the half-life of the nuclide for which the air sample had a result.

Ground air sample results were reported in units of μCi/mL and were converted to units of Bq/m^3, by a simple unit conversion.

For samples where more than one nuclide was measured in the ground air sample, the individual expected net count rates associated with each result were calculated and added and then compared to the measured aerial gamma count rate.

To compare the ground air samples to the net aerial gamma count rate, Equation 3 was used to convert the cps measured in the air into Bq/m^3. Once both the ground and aerial measurements were in the same units, the ground measurement was divided by the aerial measurement to show the comparison.

$$C_{A_i} = \frac{\dot{R}}{V \times \varepsilon_i \times Y_i} \quad [3]$$

Where:
$C_{A_i} = activity\ concentration\ (nuclide\ specific)$ (Bq/m^3)
$\dot{R} = net\ gamma\ count\ rate\ (cps)$
$V = volume\ of\ air\ surrounding\ the\ aircraft, as\ modeled\ in\ MCNP$ (m^3)
$\varepsilon_i = modeled\ efficiency\ of\ the\ NaI(Tl) detector\ pod\ used\ to\ obtain\ aerial\ gamma\ count\ rate\ (nuclide\ specific)$
$Y_i = branching\ ratio\ associated\ with\ nuclide\ of\ interest$

To determine the expected net count rate based upon the decay-corrected activity concentration measured in the ground air samples, Equation 4 was used.

$$Expected\ net\ count\ rate_i = C_{A_i} \times V \times \varepsilon_i \times Y_i \quad [4]$$

Where:
$C_{A_i} = decay - corrected\ activity\ concentration\ as\ measured\ by\ the\ ground\ air\ sample\ (nuclide\ specific)$ (Bq/m^3)
$V = volume\ of\ air\ surrounding\ the\ aircraft, as\ modeled\ in\ MCNP$
$\varepsilon_i = modeled\ efficiency\ of\ the\ NaI(Tl) detector\ pod\ used\ to\ obtain\ aerial\ gamma\ count\ rate\ (nuclide\ specific)$
$Y_i = branching\ ratio\ associated\ with\ nuclide\ of\ interest$

To determine the activity measured as ground deposition, Equation 5 was used to convert the measured net aerial count rate in cps into Bq/m^2. The results obtained with Equation 5 provide the activity concentration on the ground that would account for the aerial net gamma count rate measured.

$$C_{A_i} = \frac{\dot{R}}{A \times \varepsilon_i \times Y_i} \quad [5]$$

Where:
$C_{A_i} = activity\ concentration\ (nuclide\ specific)$ (Bq/m^2)
$\dot{R} = net\ gamma\ count\ rate\ (cps)$
$A = area\ of\ ground\ in\ the\ field\ of\ view\ of\ the\ aircraft\ during\ measurement$ (m^2)
$\varepsilon_i = modeled\ efficiency\ of\ the\ NaI(Tl) detector\ pod\ used\ to\ obtain\ aerial\ gamma\ count\ rate\ (nuclide\ specific)$
$Y_i = branching\ ratio\ associated\ with\ nuclide\ of\ interest$

In order to relate the activity concentration in terms of the three nuclides of concern, the ratio of the three nuclides found needed to be determined. Based upon the ground air samples evaluated for this project, where all three nuclides were measured, the ratio of activity concentrations was calculated to be 1% each for ^{134}Cs and ^{137}Cs and 98% ^{131}I. These measurements were taken during the period 20-23 March, which is in a

relatively short period of time following the releases from the power plant, which would also account for the higher ratio of ^{131}I, but still reasonable to be used for this analysis. These percentages were used to scale the total activity concentration attributable to each nuclide and related detector efficiency for use in equation 5. It is noted that there are varying reports on activity concentrations measured in Fukushima Prefecture following the FDNPP disaster, but these findings are in line with published findings, specifically those reported by Thakur, Ballard and Nelson. (2013)

RESULTS

The paired ground air samples were an average of 207 meters from the aerial survey point from which they were compared to, which is well within the FOV of the survey flights. The average height above earth altitude for the data points compared during this project was 623 meters.

The measured activity concentrations in units of Bq/m^3 from the ground air samples were compared to the expected activity concentration, also given in units of Bq/m^3, as calculated with Equation 4. Table 5 depicts the results from those ground air samples with measurable results (those which exceeded 0 or were above the MDA of the detection system) for all three nuclides of interest.

Table 5: Comparison of decay-corrected ground air samples with representative results for ^{134}Cs, ^{137}Cs, and ^{131}I, compared to calculated activity concentrations of net aerial gamma count rates. Note that the dashed lines in the table represent non-detectable results and that the calculated averages omit this number from consideration.

Ground Sample ID	Decay-corrected Measured Ground Air Activity Concentration (Bq/m^3)	Calculated Aerial Activity Concentration (Bq/m^3)	Comparison of Ground vs. Aerial Activity Concentrations
SCF-00003	1.482	296.77	0.50%
SCF-00057	7.734	1385.09	0.56%
SCF-00058	14.068	1385.09	1.02%
SCF-00061	5.423	1388.05	0.40%
SCF-00065	1.849	-	-
SCF-00092	2101.790	91493.81	2.30%
SCF-00093	652.801	88672.39	0.74%
SCF-00094	588.431	74275.15	0.79%
SCF-00096	172.407	38935.85	0.44%
SCF-00139	130.956	71268.34	0.18%
SCF-00140	101.633	71110.87	0.14%
SCF-00142	27.216	47377.63	0.06%
SCF-00516	0.125	30846.58	0.0004%
SCF-08991	50.482	30011.03	0.17%
Average:	275.46	42188.20	0.56%

Appendix D shows the complete results for all samples not represented in Table 5.

Table 5 demonstrates that the measured activity concentration attributable to radioactive contamination in the air as measured in ground air samples accounted for an average of 0.56% of the calculated aerial activity concentration.

The findings of the MCNP detector efficiency for each nuclide of interest for ground deposition produced the graph depicted in Figure 4 for the modeled flight altitudes of 100, 200, 350, and 550 meters

above ground. The detectors efficiency changes with altitude because the further a particle has to travel to reach the detector, the less likely it is to interact and be detected. The overall uncertainty of the efficiency of the detector for each of the nuclides varied based upon flight altitude, with the least amount of uncertainty being at the lower elevations and the most uncertainty being at the highest elevations. For instance, ^{131}I had the widest difference between the uncertainty at different elevations and ranged from 0.5% uncertainty at 100 m up to 14.6% uncertainty at 550 m. Based on Figure 4, it can be seen that the detectors are slightly more efficient at measuring emissions from a ^{134}Cs source than ^{137}Cs and ^{131}I, at all altitudes, with the difference in efficiencies remaining relatively constant through all modeled altitudes.

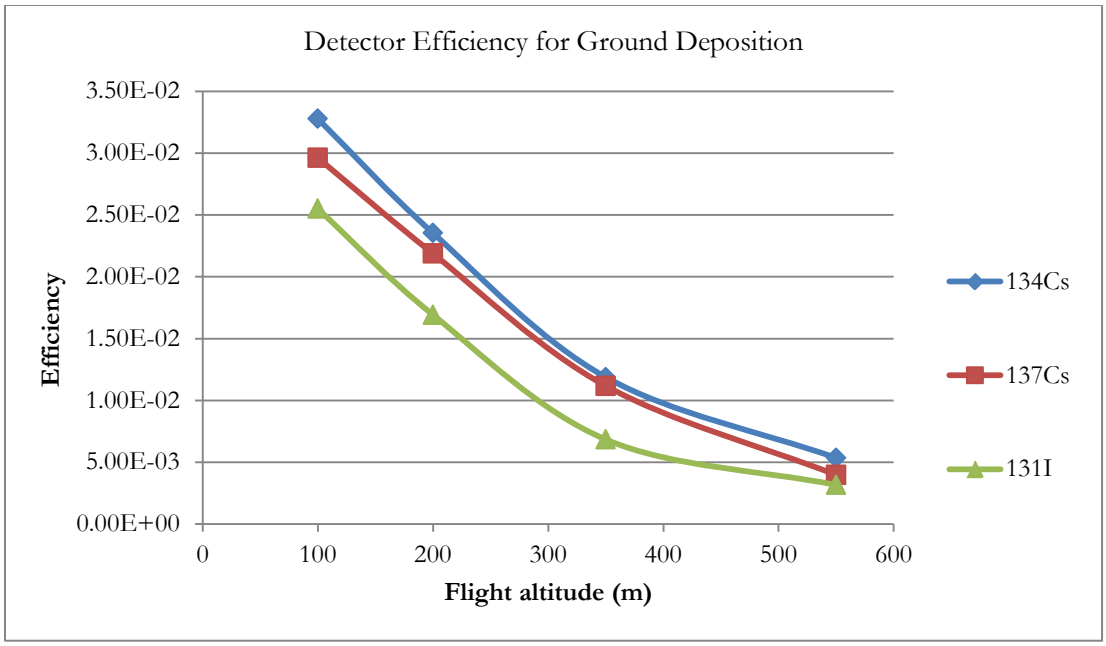

Figure 4: Detector pod efficiency for measuring ground deposition based upon nuclide and flight altitude (m).

Additional analysis was conducted to compare the aerial net gamma count rate measurements void of the ground air sample measurements, the result is an estimate of the ground deposition that would have been measured during the aerial survey flights, but not detected in the ground air measurements due to the fact that the radioactivity would no longer be airborne, but rather be deposited onto the ground surface. Table 6 represents the estimated ground deposition for those ground air samples with positive results for all three nuclides of interest.

Table 6: Estimated ground deposition calculated from measured aerial net gamma count rate minus the expected net count rate based upon the measured ground air samples, inclusive of the ground air samples with representative results for ^{134}Cs, ^{137}Cs, and ^{131}I. Note that the dashed lines in the table represent non-detectable results and the calculated averages omit this number from consideration.

Ground Sample ID	Expected Net Count Rate Based on Ground Air Sample (s^{-1})	Actual Net Count Rate Minus Expected Net Count Rate (s^{-1})	Net Counts Divided by Area Covered by Aircraft (cps/m^2)	Estimated Ground deposition (Bq/m^2)
SCF-00003	1.83	361.22	0.00031	2.98E+06
SCF-00057	9.47	1684.93	0.0014	1.23E+07
SCF-00058	17.33	1677.07	0.0014	1.23E+07
SCF-00061	6.80	1691.22	0.00079	2.48E+07
SCF-00065	2.27	-	-	-
SCF-00092	2571.407	109354.13	0.66	2.67E+05
SCF-00093	797.34	107676.69	0.62	2.79E+05
SCF-00094	719.777	90141.96	0.24	7.67E+05
SCF-00096	211.00	47419.72	0.22	4.95E+05
SCF-00139	160.76	87022.70	0.53	2.93E+05
SCF-00140	124.57	86866.25	0.53	2.97E+05
SCF-00142	33.29	57924.37	0.042	9.11E+06
SCF-00516	0.15	37734.85	0.11	9.46E+05
SCF-08991	64.64	36648.23	0.11	9.37E+05
Average:	337.19	51246.41	0.24	5.40E+06

Appendix E shows the complete results for all samples not represented in Table 6.

Table 6 demonstrates that the ground deposition after the removal of the measured activity concentration in the air and the measured aerial gamma count rate averaged 5.4E6 Bq/m^2 over the field of view of the aircraft, which averages an area of 0.66 km^2 for the evaluated measurements in Table 6.

There were also 17 different ground air samples which did not detect any measurable amount of any of the three nuclides of interest, but were matched to appropriate aerial gamma count rate measurements. Table 7 depicts those samples and the estimated ground radiation contamination, based on the supposition that all measured aerial gamma count rate would be due to ground deposition since the presence of air contamination was not detected.

Table 7: Estimated ground deposition calculated from measured aerial net gamma count rate, adjusted to ground level, for the ground air samples with non-detectable results for ^{134}Cs, ^{137}Cs, and ^{131}I. Note that the dashed lines in the table represent non-detectable results and the calculated averages omit this number from consideration.

Ground Sample ID	Collection Date	Gross count rate (cps)	Net Count Rate (cps)	Activity concentration based on Net Count Rate (Bq/m²)	Ground deposition (Bq/m²)
SCF-00050	19-Mar-11	45201.32	39019.96	10060.42	5.50E+05
SCF-00625	9-May-11	4323.46	-	-	-
SCF-00625C	9-May-11	4323.46	-	-	-
SCF-00627	9-May-11	4187.21	-	-	-
SCF-00627C	9-May-11	4187.21	-	-	-
SCF-00629	9-May-11	13865.86	7684.50	1981.276	4.02E+05
SCF-00629C	9-May-11	14003.84	7822.48	2016.85	4.10E+05
SCF-00631	9-May-11	14556.42	8375.06	2159.321	4.43E+05
SCF-00633	9-May-11	11712.49	5531.13	1426.077	2.62E+05
SCF-00633C	9-May-11	11756.69	5575.33	1437.474	2.63E+05
SCF-00635	9-May-11	11211.72	5030.37	1296.967	2.39E+05
SCF-00635C	9-May-11	11133.01	4951.65	1276.672	2.35E+05
SCF-08666	2-Apr-11	6579.09	397.73	102.5462	4.21E+04
SCF-08832	10-May-11	1947.30	-	-	-
SCF-08832C	10-May-11	1878.29	-	-	-
SCF-08834	10-May-11	18009.3	11827.95	3049.569	6.56E+05
SCF-08834C	10-May-11	18113.23	11931.88	3076.366	6.64E+05
Average:		11587.64	9831.64	2534.87	3.79E+05

Table 7 demonstrates that the activity concentration attributable to ground deposition calculated from the measured net aerial gamma count rate averaged 3.79E5 Bq/m² for the measurements with finite net count rates in the detectors over the field of view of the aircraft, which averages an area of 1.6 km² for the evaluated measurements in Table 7. The average reported excludes six measurements which did not result in a finite net count rate, so the average only represents the remaining eleven samples.

A comparison of the average total ground deposition calculated from aerial measurements where there was detectable activity concentration of ^{134}Cs, ^{137}Cs, and ^{131}I to those aerial measurements where there was not any detectable activity of those nuclides shows a difference of a factor of 14.25. Thus indicating that there was approximately 14.25 times more ground deposition in areas where there was measurable activity concentration of ^{134}Cs, ^{137}Cs, and ^{131}I, versus areas where there was no detectable activity concentration of those nuclides.

DISCUSSION

The comparison of ground air samples to aerial gamma count rate shows an average difference of one and a half orders of magnitude. This is an expected finding when factors like the timeline of events following the FDNPP accident along with weather patterns and the nature of ground deposition from an event such as this are considered. While every effort to compare the ground air sample to an aerial gamma measurement obtained at the same time, the fact is that the average time in between paired samples was just over four days and although that time frame can be accounted for as far as the decay of measured nuclides, the potential for changes in wind and weather can alter the measured air and ground activity concentrations. Such weather factors as rainout and washout of particulate in the air as well as movement of ground deposition by wind and rain, both typical weather patterns in Japan, also contribute to this variability. Pooling of nuclides in locations other than where they were originally deposited can occur, although it is more likely that dramatic changes would take a more considerable amount of time than the average of four days in between samples, it could still account for part of this difference.

Saito, et al. published their study of soil samples collected from Fukushima Prefecture for the time period 4 June-8 July 2011 and their findings are consistent with the calculated ground depositions of this project. (Saito, et al., 2014) While their methods included direct measurement of the soil obtained from Fukushima Prefecture and this project was based upon relating ground air samples and AGS data, the fact that Saito, et al's findings are consistent with this project gives more strength to the methods used in this project.

The significance of the data in Table 7, the estimated ground deposition determined by the aerial net gamma count measurement in locations where there were no measurable nuclides in the ground air samples, is that it represents the radioactivity of ground deposition as measured from the aerial surveys. This proves beneficial to responders in that it helps to concentrate efforts for remediation following an accident such as FDNPP.

It is important to note that one significant difference between ^{131}I and ^{134}Cs and ^{137}Cs is that ^{131}I is a vapor and is best sampled using a charcoal filter when air sampling is the method used for detection. We were

not able to identify with certainty which individual filter media were used during the air sample collection during the response to the FDNPP accident.

There has been research into the actual nuclide ratios measured following the FDNPP accident and the use of the actual ratios measured in this project is a viable method for determining estimated ground deposition based upon net aerial gamma count rate, but knowing the actual nuclide ratio for the location this method is applied to would also strengthen the results of this project, especially for samples without a measured ground air sample showing the ratio. The nuclide ratios measured in the ground air samples used in this project are consistent with the ranges found in other research projects, specifically those reported by Thakur, Ballard, and Nelson. (2013)

The data used for this project was the fundamental output of the detectors with only minimal processing by default routines and had not been corrected for background, altitude, decay, or detector efficiency. Since virtually no processing had been performed on the data since its collection, it provided an open path to interpretation and analysis. It also provided the opportunity to interpret the data and make educated assumptions about it. Without knowing the actual background radiation measurement for the area being surveyed, applying the method used by the survey team to the unprocessed data provided an adequate background measurement, but knowing the actual value would strengthen the results of this project.

The aerial gross gamma count measurements used for this project were from parameters set by the manufacturer, not by AMS, which could influence the strength of the data, since the known window or parameters set to collect these data points is not known by AMS or this project team. RSI, the detector manufacturer is a leader in their industry, so assuming factory defaults are reasonable is a good assumption, but does leave room for error or unexpected exclusion of data.

Only the efficiency of one detector pod was modeled, because it was reported that some survey flights only had one pod, but as many as three pods may have been used during an individual survey flight, making the overall efficiency of the system better and this analysis representative of the lower end of the spectrum of system efficiencies.

Another assumption made that could influence the strength of the findings of this project is the modeled efficiency of the detectors used, rather than having the actual detector efficiency. MCNP has been a proven tool to estimate the efficiency of a detector, but having the actual efficiency is preferred and would also strengthen the results. Using MCNP to model detector efficiency for aerial radiation measurements was a proven method used by Sinclair et al. to determine radioxenon concentrations following the FDNPP accident (Sincalir, et al., 2011) The MCNP models used to determine the efficiency of the detector are basic in nature and reflect the actual size of each NaI(Tl) crystal, but do not take into account other factors such as detector or aircraft components that would affect the real efficiency of the detector.

CONCLUSION

The importance of this study is that it could provide a basis for differentiating between ground air samples and aerial gamma count rate measurements. This details a method used to characterize the expected ground deposition based upon the net gamma count rate observed. The advantage of this is to help provide a map for emergency responders and remediation teams to focus their efforts on areas which require a greater level of personal protective gear to prevent further contamination and remediation.

The calculated and modeled ground deposition in Fukushima Prefecture as determined from this project shows an estimated ground deposition of averaged 3.79E5 Bq/m^2, with the major contribution coming from ^{131}I, based on the measured activity concentrations in air for this time period and location. The significance of the majority being from ^{131}I is that with its eight day half-life, the majority of ground deposition would now be considered to be decayed away. This shows the importance of knowing not only the nuclide ratios that are being surveyed, but also their half-lives, the way they move in the environment, and their activity concentration. If the ratio were reversed and the majority of ground deposition was from ^{137}Cs, with its 30 year half-life, then there would still be a considerable amount of that nuclide in those areas and additional precautions would need to be evaluated.

The main sources of uncertainty of the findings of this project are related to where assumptions were made in the place of actual data. For instance modeling the detector efficiency instead of knowing the actual measured detector efficiency lends a level of uncertainty to the project. Also assuming the gross gamma count rate used for data analysis was from an open window of detection and not knowing this creates additional uncertainty in the findings, but the same assumption was applied across the project, thus the overall findings should account for the same level of uncertainty and not create a level of overall bias.

The methods used in this project could be applied to other scenarios with the same assumptions, but moving forward, ensuring the measurements are performed with set parameters for different energy channels and the efficiency of the detector known, the strength of the findings would be more certain. The different energy channels would make identification of specific nuclides easier and potentially much quicker, enabling recommendations to be made to emergency responders in a timely manner and with better guidance for

personal protection based upon the requirements for each type of nuclide present, in the case of an accident, such as FDNPP.

Future work:

The vast amount of data collected in response to the FDNPP accident lends itself to a wealth of possibilities in future research and analysis. I would recommend trying to locate ground soil samples in the areas where the estimated ground deposition was calculated to compare the findings of this project.

REFERENCES

Baba, M. (2013). Fukushima accident: What happened? *Radiation Measurements , 55*, 17-21.

Bartlett, D. (2007, January 7). *A Practical Guide to GPS - UTM*. Retrieved April April, 2014, from http://www.dbartlett.com/

Blumenthal, D. J., Bowman, D. R., & Remick, A. (2012, May). Adapting the U.S. domestic radiological emergency response process to an overseas incident: FRMAC without the F. *Health Physics*, 485-488.

Caciolli, A., Baldoncini, M., Bezzon, G. P., Broggini, C., Buso, G. P., Callegari, I., et al. (2012). A new FSA approach for in situ gamma ray spectroscopy. *Science of the Total Environment*, 639-645.

Cember, H., & Johnson, T. E. (2009). *Introduction to Health Physics* (Fourth ed.). United States: McGraw-Hill.

Cresswell, A. J., & Sanderson, D. C. (2012). Evaluating airborne and ground based gamma spectrometry methods for detecting particulate radioactivity in the environment: A case study of Irish Sea Beaches. *Science of the Total Environment* , 285-296.

Fujiwara, T., Saito, T., Muroya, Y., Sawahata, H., Yamashita, Y., Nagasaki, S., et al. (2012). Isotopic ratio and vertical distribution of radionuclides in soil affected by the accident of Fukushima Dai-ichi nuclear power plants. *Journal of Environmental Radioactivity* , 37-44.

Johnson, T. E., & Birky, B. K. (2012). *Health Physics and Radiological Health.* Baltimore, MD: Lippincott Williams & Wilkins.

Kalos, M. H., & Whitlock, P. A. (2008). *Monte Carlo Methods.* Great Britian: Wiley-VCH.

Kluson, J. (2010). In-situ gamma spectrometry in environmental monitoring. *Applied Radiation and Isotopes, 68*, 529-535.

Knoll, G. F. (2010). *Radiation Detection and Measurement* (4th ed.). Hoboken, NJ: Wiley.

Kock, P., & Samuelsson, C. (2011). Comparison of airborne and terrestrial gamma spectrometry measurements - evaluation of three areas in souther Sweden. *Journal of Environmental Radioactivity*, 605-613.

Kortov, V., & Ustyantsev, Y. (2013). Chernobyl accident: Causes, consequences and problems of radiation measurements. *Radiation Measurements* , 12-16.

Lyons, C., & Colton, D. (2012). Aerial measuring system in Japan. *Health Physics, 102* (5), 509-515.

Mena, R., Pemberston, W., & Beal, W. (2012). Emergency response health physics. *Health Physics , 102* (5), 542-548.

Nuccetelli, C. (2008). In situ gamma spectroscopy in environmental research and monitoring. *Applied Radiation and Isotopes , 66*, 1615-1618.

Sanderson, D. C., Cresswell, A. J., Hardeman, F., & Debauche, A. (2004). An airborne gamma-ray spectrometry survey of nuclear sites in Belgium. *Journal of Environmental Radioactivity*, 213-224.

Smith, A. (2013, September 10). *Fukushima evacuation has killed more than earthquake and tsunami, survey says*. Retrieved May 17, 2014, from NBC News: http://www.nbcnews.com/news/other/fukushima-evacuation-has-killed-more-earthquake-tsunami-survey-says-f8C11120007

Steinhauser, G., Brandl, A., & Johnson, T. E. (2014). Comparison of the Chernobyl and Fukushima nuclear accidents: A review of the environmental impacts. *Science of the Total Environment*, 800-817.

Terada, H., Katata, G., Chino, M., & Nagai, H. (2012). Atmospheric discharge and dispersion of radionuclides during the Fukushima Dai-ichi Nuclear Power Plant accident. Part II: Verification of the source term and analysis of regional-scale atmospheric dispersion. *Journal of Environmental Radioactivity*, 141-154.

Thakur, P., Ballard, S., & Nelson, R. (2013). An overview of Fukushima radionuclides measured in the northern hemisphere. *Science of the Total Environment*, 577-613.

Tracy, B. L., Carini, F., Barabash, S., Berkovskyy, V., Brittain, J. E., Chouhan, S., et al. (2013). The sensitivity of different environmnets to radioactive contamination. *Journal of Environmental Radioactivity , 122*, 1-8.

VanHorne-Sealy, J., Livingston, B., & Al, L. (2012). DoD's Medical Radiobiological Advisory Team: Experts on the ground. *Health Physics Society, 102* (5), 489-492.

Wershofen, H. (2013). Remarks on representative ground-level air monitoring. *Applied Radiation and Isotopes*, 284-289.

Winkelmann, I., Strobl, C., & Thomas, M. (2004). Aerial measurements of artificial radionuclides in Germany in case of a nuclear accident. *Journal of Environmental Radioactivity* , 225-231.

World Nuclear Association. (2014, April 22). *Fukushima Accident*. Retrieved May 17, 2014, from World Nuclear Association: http://www.world-nuclear.org/info/safety-and-security/safety-of-plants/fukushima-accident/

APPENDIX A: ARCMAP SCREEN SHOTS OF DATA POINTS FROM AMS AERIAL SURVEY FLIGHTS.

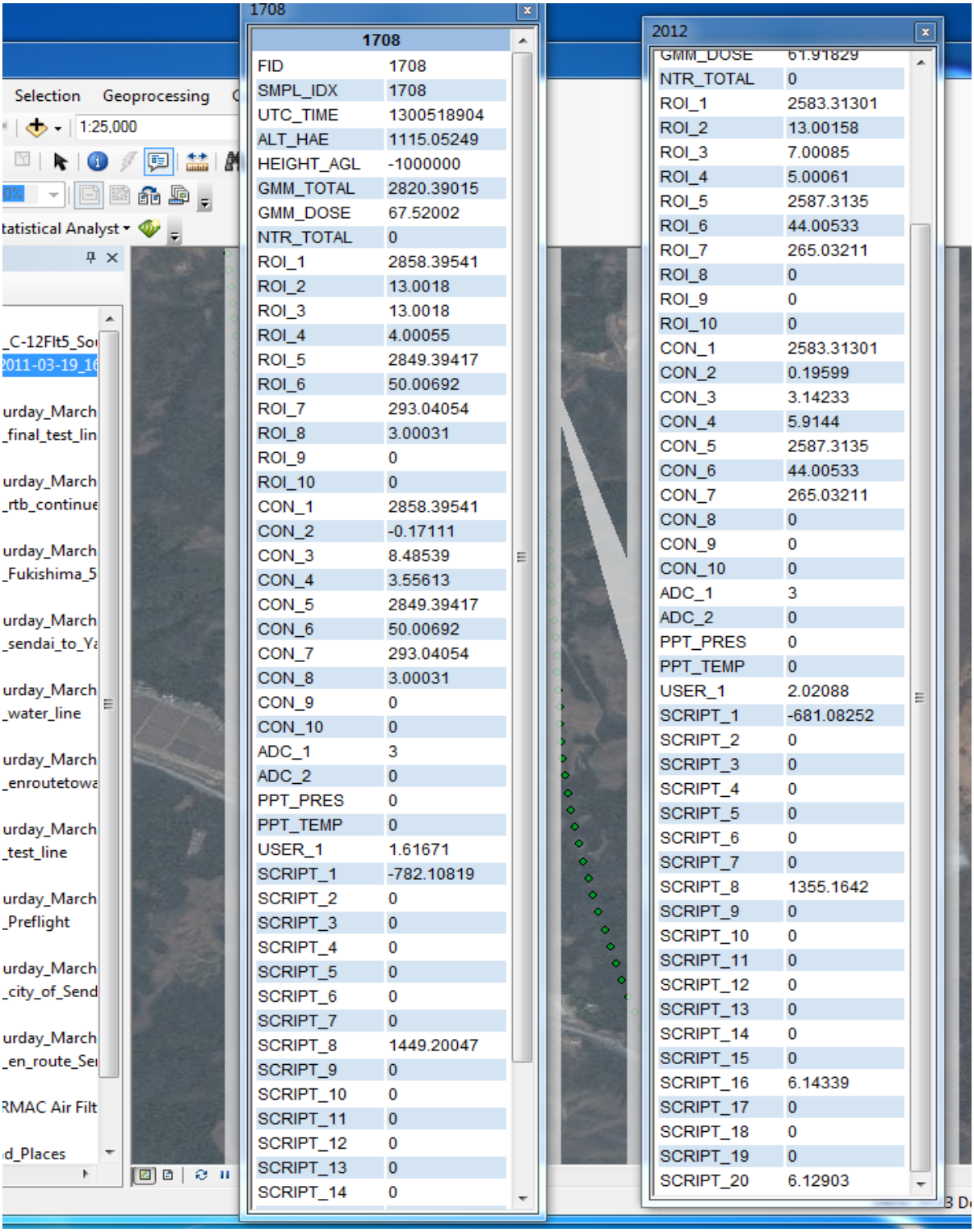

1708

1708	
FID	1708
SMPL_IDX	1708
UTC_TIME	1300518904
ALT_HAE	1115.05249
HEIGHT_AGL	-1000000
GMM_TOTAL	2820.39015
GMM_DOSE	67.52002
NTR_TOTAL	0
ROI_1	2858.39541
ROI_2	13.0018
ROI_3	13.0018
ROI_4	4.00055
ROI_5	2849.39417
ROI_6	50.00692
ROI_7	293.04054
ROI_8	3.00031
ROI_9	0
ROI_10	0
CON_1	2858.39541
CON_2	-0.17111
CON_3	8.48539
CON_4	3.55613
CON_5	2849.39417
CON_6	50.00692
CON_7	293.04054
CON_8	3.00031
CON_9	0
CON_10	0
ADC_1	3
ADC_2	0
PPT_PRES	0
PPT_TEMP	0
USER_1	1.61671
SCRIPT_1	-782.10819
SCRIPT_2	0
SCRIPT_3	0
SCRIPT_4	0
SCRIPT_5	0
SCRIPT_6	0
SCRIPT_7	0
SCRIPT_8	1449.20047
SCRIPT_9	0
SCRIPT_10	0
SCRIPT_11	0
SCRIPT_12	0
SCRIPT_13	0
SCRIPT_14	0

2012

GMM_DOSE	61.91829
NTR_TOTAL	0
ROI_1	2583.31301
ROI_2	13.00158
ROI_3	7.00085
ROI_4	5.00061
ROI_5	2587.3135
ROI_6	44.00533
ROI_7	265.03211
ROI_8	0
ROI_9	0
ROI_10	0
CON_1	2583.31301
CON_2	0.19599
CON_3	3.14233
CON_4	5.9144
CON_5	2587.3135
CON_6	44.00533
CON_7	265.03211
CON_8	0
CON_9	0
CON_10	0
ADC_1	3
ADC_2	0
PPT_PRES	0
PPT_TEMP	0
USER_1	2.02088
SCRIPT_1	-681.08252
SCRIPT_2	0
SCRIPT_3	0
SCRIPT_4	0
SCRIPT_5	0
SCRIPT_6	0
SCRIPT_7	0
SCRIPT_8	1355.1642
SCRIPT_9	0
SCRIPT_10	0
SCRIPT_11	0
SCRIPT_12	0
SCRIPT_13	0
SCRIPT_14	0
SCRIPT_15	0
SCRIPT_16	6.14339
SCRIPT_17	0
SCRIPT_18	0
SCRIPT_19	0
SCRIPT_20	6.12903

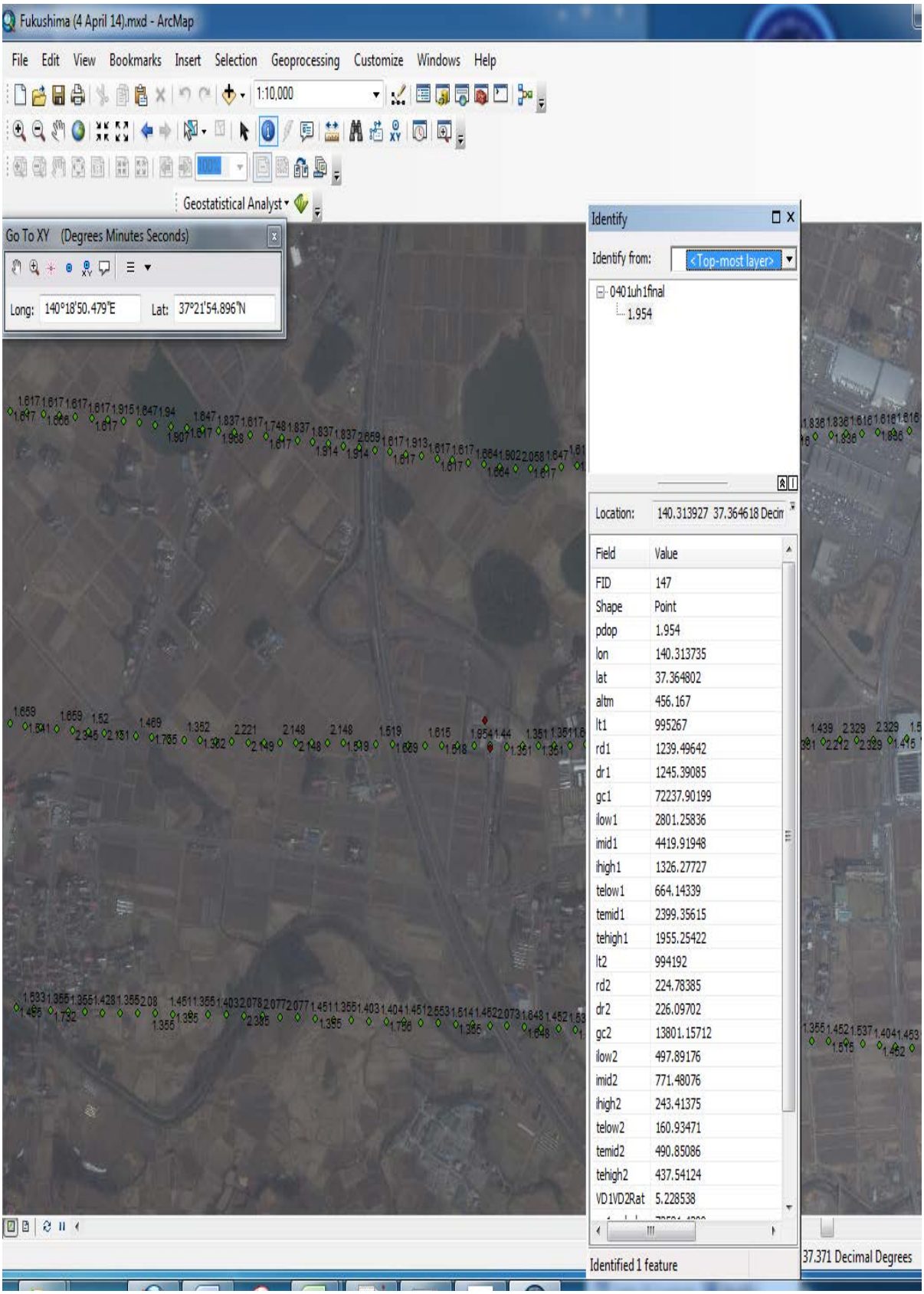
Fukushima (4 April 14).mxd - ArcMap
File Edit View Bookmarks Insert Selection Geoprocessing Customize Windows Help
1:10,000
Geostatistical Analyst
Go To XY (Degrees Minutes Seconds)
Long: 140°18'50.479"E
Lat: 37°21'54.896"N
Identify
Identify from: <Top-most layer>
0401uh1final
1.954
Location: 140.313927 37.364618 Decim
Field Value
FID 147
Shape Point
pdop 1.954
lon 140.313735
lat 37.364802
altm 456.167
lt1 995267
rd1 1239.49642
dr1 1245.39085
gc1 72237.90199
ilow1 2801.25836
imid1 4419.91948
ihigh1 1326.27727
telow1 664.14339
temid1 2399.35615
tehigh1 1955.25422
lt2 994192
rd2 224.78385
dr2 226.09702
gc2 13801.15712
ilow2 497.89176
imid2 771.48076
ihigh2 243.41375
telow2 160.93471
temid2 490.85086
tehigh2 437.54124
VD1VD2Rat 5.228538
Identified 1 feature
37.371 Decimal Degrees

APPENDIX B: MCNP MODEL FOR AMS DETECTOR EFFICIENCY FOR SUBMERSION SOURCE

```
c Thesis detector efficiency
c Cell Cards
1     2 -3.67 -3                          $NaI detector 1
2     2 -3.67 -5                          $NaI detector 2
3     2 -3.67 -7                          $NaI detector 3
4     1 -0.0012048 2 4 6 -8               $air space
45    1 -0.0012048 9 -1                   $air space to break up cell 4
5     3 -2.7 -2 3                         $Al casing around detector 1
6     3 -2.7 -4 5                         $Al casing around detector 2
7     3 -2.7 -6 7                         $Al casing around detector 3
8     3 -2.7 8 -9                         $Al aircraft skin
9     0 1                                 $universe

c Surface Card
1     so 2500                             $sphere about origin with 25 m radius
2     rpp -0.1 5.1 -0.1 10.1 -0.1 40.1    $2mm thick Al casing around detector
3     rpp 0 5 0 10 0 40                   $NaI detector 5 cm x 10 cm x 40 cm
4     rpp 6.1 11.3 -0.1 10.1 -0.1 40.1    $2mm thick Al casing around detector
5     rpp 6.2 11.2 0 10 0 40              $NaI detector 5 cm x 10 cm x 40 cm
6     rpp 12.3 17.5 -0.1 10.1 -0.1 40.1   $2mm thick Al casing around detector
7     rpp 12.4 17.4 0 10 0 40             $NaI detector 5 cm x 10 cm x 40 cm
8     so 100                              $sphere of air around detector
9     so 100.3                            $sphere replicating aircraft

c Data Cards
c Source Homogeneous Distribution of nuclide in air
c sdef pos=0 0 0 rad=d1 erg=0.662 par=2 $source definition for Cs-137
c sdef pos=0 0 0 rad=d1 erg=d2 par=2    $source definition for Cs-134
sdef pos=0 0 0 rad=d1 erg=d2 par=2      $source definition for I-131
si1 100.3 2499                          $spherical source located outside aircraft
sp1 -21 2
c si2 l 0.605 0.796                     $Cs-134 energies
c sp2 0.6853 0.2333
si2 l 0.284 0.364 0.637                 $I-131 energies
sp2 0.0548 0.730 0.00487
mode p                                  $photons
imp:p 1 1 1 1 1 1 1 1 1 0               $all cells with importance of 1, except universe
nps  500000000
m1   007014 -0.7553                     $air density = 0.0012048 g/cm^3
     008016 -0.2318
     018000 -0.01282
     006012 -0.000125
m2   011000 -0.5                        $NaI density 3.67 g/cm^3
     053000 -0.5
m3   013000 -1                          $Al density 2.7 g/cm^3
c F8 Tally energy deposition
F18:p 1                                 $detector 1
#   E18
    0
```

```
   0.010
   0.500
   0.700
   10
F28:p 2                                $detector 2
#   E28
   0
   0.010
   0.500
   0.700
   10
F38:p 3                                $detector 3
#   E38
   0
   0.010
   0.500
   0.700
   10
```

APPENDIX C: MCNP MODEL FOR AMS DETECTOR EFFICIENCY OF GROUND DEPOSITION

```
c Thesis detector efficiency
c Cell Cards
142   2 -3.67 -142 imp:p=1        $NaI detector 14a
144   2 -3.67 -144 imp:p=1        $NaI detector 14b
146   2 -3.67 -146 imp:p=1        $NaI detector 14c
112   2 -3.67 -112 imp:p=1        $NaI detector 11a
114   2 -3.67 -114 imp:p=1        $NaI detector 11b
116   2 -3.67 -116 imp:p=1        $NaI detector 11c
122   2 -3.67 -122 imp:p=1        $NaI detector 12a
124   2 -3.67 -124 imp:p=1        $NaI detector 12b
126   2 -3.67 -146 imp:p=1        $NaI detector 12c
132   2 -3.67 -132 imp:p=1        $NaI detector 13a
134   2 -3.67 -134 imp:p=1        $NaI detector 13b
136   2 -3.67 -136 imp:p=1        $NaI detector 13c
152   2 -3.67 -152 imp:p=1        $NaI detector 15a
154   2 -3.67 -154 imp:p=1        $NaI detector 15b
156   2 -3.67 -156 imp:p=1        $NaI detector 15c
162   2 -3.67 -162 imp:p=1        $NaI detector 16a
164   2 -3.67 -164 imp:p=1        $NaI detector 16b
166   2 -3.67 -166 imp:p=1        $NaI detector 16c
172   2 -3.67 -172 imp:p=1        $NaI detector 17a
174   2 -3.67 -174 imp:p=1        $NaI detector 17b
176   2 -3.67 -176 imp:p=1        $NaI detector 17c
182   2 -3.67 -182 imp:p=1        $NaI detector 18a
184   2 -3.67 -184 imp:p=1        $NaI detector 18b
186   2 -3.67 -186 imp:p=1        $NaI detector 18c
242   2 -3.67 -242 imp:p=1        $NaI detector 24a
244   2 -3.67 -244 imp:p=1        $NaI detector 24b
246   2 -3.67 -246 imp:p=1        $NaI detector 24c
212   2 -3.67 -212 imp:p=1        $NaI detector 21a
214   2 -3.67 -214 imp:p=1        $NaI detector 21b
216   2 -3.67 -216 imp:p=1        $NaI detector 21c
222   2 -3.67 -222 imp:p=1        $NaI detector 22a
224   2 -3.67 -224 imp:p=1        $NaI detector 22b
226   2 -3.67 -226 imp:p=1        $NaI detector 22c
232   2 -3.67 -232 imp:p=1        $NaI detector 23a
234   2 -3.67 -234 imp:p=1        $NaI detector 23b
236   2 -3.67 -236 imp:p=1        $NaI detector 23c
252   2 -3.67 -252 imp:p=1        $NaI detector 25a
254   2 -3.67 -254 imp:p=1        $NaI detector 25b
256   2 -3.67 -256 imp:p=1        $NaI detector 25c
262   2 -3.67 -262 imp:p=1        $NaI detector 26a
264   2 -3.67 -264 imp:p=1        $NaI detector 26b
266   2 -3.67 -266 imp:p=1        $NaI detector 26c
272   2 -3.67 -272 imp:p=1        $NaI detector 27a
274   2 -3.67 -274 imp:p=1        $NaI detector 27b
276   2 -3.67 -276 imp:p=1        $NaI detector 27c
282   2 -3.67 -282 imp:p=1        $NaI detector 28a
284   2 -3.67 -284 imp:p=1        $NaI detector 28b
```

```
286   2 -3.67 -286 imp:p=1        $NaI detector 28c
342   2 -3.67 -342 imp:p=1        $NaI detector 34a
344   2 -3.67 -344 imp:p=1        $NaI detector 34b
346   2 -3.67 -346 imp:p=1        $NaI detector 34c
312   2 -3.67 -312 imp:p=1        $NaI detector 31a
314   2 -3.67 -314 imp:p=1        $NaI detector 31b
316   2 -3.67 -316 imp:p=1        $NaI detector 31c
322   2 -3.67 -322 imp:p=1        $NaI detector 32a
324   2 -3.67 -324 imp:p=1        $NaI detector 32b
326   2 -3.67 -326 imp:p=1        $NaI detector 32c
332   2 -3.67 -332 imp:p=1        $NaI detector 33a
334   2 -3.67 -334 imp:p=1        $NaI detector 33b
336   2 -3.67 -336 imp:p=1        $NaI detector 33c
352   2 -3.67 -352 imp:p=1        $NaI detector 35a
354   2 -3.67 -354 imp:p=1        $NaI detector 35b
356   2 -3.67 -356 imp:p=1        $NaI detector 35c
362   2 -3.67 -362 imp:p=1        $NaI detector 36a
364   2 -3.67 -364 imp:p=1        $NaI detector 36b
366   2 -3.67 -366 imp:p=1        $NaI detector 36c
372   2 -3.67 -372 imp:p=1        $NaI detector 37a
374   2 -3.67 -374 imp:p=1        $NaI detector 37b
376   2 -3.67 -376 imp:p=1        $NaI detector 37c
382   2 -3.67 -382 imp:p=1        $NaI detector 38a
384   2 -3.67 -384 imp:p=1        $NaI detector 38b
386   2 -3.67 -386 imp:p=1        $NaI detector 38c
442   2 -3.67 -442 imp:p=1        $NaI detector 44a
444   2 -3.67 -444 imp:p=1        $NaI detector 44b
446   2 -3.67 -446 imp:p=1        $NaI detector 44c
412   2 -3.67 -412 imp:p=1        $NaI detector 41a
414   2 -3.67 -414 imp:p=1        $NaI detector 41b
416   2 -3.67 -416 imp:p=1        $NaI detector 41c
422   2 -3.67 -422 imp:p=1        $NaI detector 42a
424   2 -3.67 -424 imp:p=1        $NaI detector 42b
426   2 -3.67 -426 imp:p=1        $NaI detector 42c
432   2 -3.67 -432 imp:p=1        $NaI detector 43a
434   2 -3.67 -434 imp:p=1        $NaI detector 43b
436   2 -3.67 -436 imp:p=1        $NaI detector 43c
452   2 -3.67 -452 imp:p=1        $NaI detector 45a
454   2 -3.67 -454 imp:p=1        $NaI detector 45b
456   2 -3.67 -456 imp:p=1        $NaI detector 45c
462   2 -3.67 -462 imp:p=1        $NaI detector 46a
464   2 -3.67 -464 imp:p=1        $NaI detector 46b
466   2 -3.67 -466 imp:p=1        $NaI detector 46c
472   2 -3.67 -472 imp:p=1        $NaI detector 47a
474   2 -3.67 -474 imp:p=1        $NaI detector 47b
476   2 -3.67 -476 imp:p=1        $NaI detector 47c
482   2 -3.67 -482 imp:p=1        $NaI detector 48a
484   2 -3.67 -484 imp:p=1        $NaI detector 48b
486   2 -3.67 -486 imp:p=1        $NaI detector 44c
141   3 -2.7 -141 142 imp:p=1        $Al casing around detector  14a
143   3 -2.7 -143 144 imp:p=1        $Al casing around detector  14b
145   3 -2.7 -145 146 imp:p=1        $Al casing around detector  14c
```

```
111   3 -2.7 -111 112 imp:p=1        $Al casing around detector  11a
113   3 -2.7 -113 114 imp:p=1        $Al casing around detector  11b
115   3 -2.7 -115 116 imp:p=1        $Al casing around detector  11c
121   3 -2.7 -121 122 imp:p=1        $Al casing around detector  12a
123   3 -2.7 -123 124 imp:p=1        $Al casing around detector  12b
125   3 -2.7 -125 146 imp:p=1        $Al casing around detector  12c
131   3 -2.7 -131 132 imp:p=1        $Al casing around detector  13a
133   3 -2.7 -133 134 imp:p=1        $Al casing around detector  13b
135   3 -2.7 -135 136 imp:p=1        $Al casing around detector  13c
151   3 -2.7 -151 152 imp:p=1        $Al casing around detector  15a
153   3 -2.7 -153 154 imp:p=1        $Al casing around detector  15b
155   3 -2.7 -155 156 imp:p=1        $Al casing around detector  15c
161   3 -2.7 -161 162 imp:p=1        $Al casing around detector  16a
163   3 -2.7 -163 164 imp:p=1        $Al casing around detector  16b
165   3 -2.7 -165 166 imp:p=1        $Al casing around detector  16c
171   3 -2.7 -171 172 imp:p=1        $Al casing around detector  17a
173   3 -2.7 -173 174 imp:p=1        $Al casing around detector  17b
175   3 -2.7 -175 176 imp:p=1        $Al casing around detector  17c
181   3 -2.7 -181 182 imp:p=1        $Al casing around detector  18a
183   3 -2.7 -183 184 imp:p=1        $Al casing around detector  18b
185   3 -2.7 -185 186 imp:p=1        $Al casing around detector  18c
241   3 -2.7 -241 242 imp:p=1        $Al casing around detector  24a
243   3 -2.7 -243 244 imp:p=1        $Al casing around detector  24b
245   3 -2.7 -245 246 imp:p=1        $Al casing around detector  24c
211   3 -2.7 -211 212 imp:p=1        $Al casing around detector  21a
213   3 -2.7 -213 214 imp:p=1        $Al casing around detector  21b
215   3 -2.7 -215 216 imp:p=1        $Al casing around detector  21c
221   3 -2.7 -221 222 imp:p=1        $Al casing around detector  22a
223   3 -2.7 -223 224 imp:p=1        $Al casing around detector  22b
225   3 -2.7 -225 226 imp:p=1        $Al casing around detector  22c
231   3 -2.7 -231 232 imp:p=1        $Al casing around detector  23a
233   3 -2.7 -233 234 imp:p=1        $Al casing around detector  23b
235   3 -2.7 -235 236 imp:p=1        $Al casing around detector  23c
251   3 -2.7 -251 252 imp:p=1        $Al casing around detector  25a
253   3 -2.7 -253 254 imp:p=1        $Al casing around detector  25b
255   3 -2.7 -255 256 imp:p=1        $Al casing around detector  25c
261   3 -2.7 -261 262 imp:p=1        $Al casing around detector  26a
263   3 -2.7 -263 264 imp:p=1        $Al casing around detector  26b
265   3 -2.7 -265 266 imp:p=1        $Al casing around detector  26c
271   3 -2.7 -271 272 imp:p=1        $Al casing around detector  27a
273   3 -2.7 -273 274 imp:p=1        $Al casing around detector  27b
275   3 -2.7 -275 276 imp:p=1        $Al casing around detector  27c
281   3 -2.7 -281 282 imp:p=1        $Al casing around detector  28a
283   3 -2.7 -283 284 imp:p=1        $Al casing around detector  28b
285   3 -2.7 -285 286 imp:p=1        $Al casing around detector  28c
341   3 -2.7 -341 342 imp:p=1        $Al casing around detector  34a
343   3 -2.7 -343 344 imp:p=1        $Al casing around detector  34b
345   3 -2.7 -345 346 imp:p=1        $Al casing around detector  34c
311   3 -2.7 -311 312 imp:p=1        $Al casing around detector  31a
313   3 -2.7 -313 314 imp:p=1        $Al casing around detector  31b
315   3 -2.7 -315 316 imp:p=1        $Al casing around detector  31c
321   3 -2.7 -321 322 imp:p=1        $Al casing around detector  32a
```

```
323   3 -2.7 -323 324 imp:p=1          $Al casing around detector  32b
325   3 -2.7 -325 326 imp:p=1          $Al casing around detector  32c
331   3 -2.7 -331 332 imp:p=1          $Al casing around detector  33a
333   3 -2.7 -333 334 imp:p=1          $Al casing around detector  33b
335   3 -2.7 -335 336 imp:p=1          $Al casing around detector  33c
351   3 -2.7 -351 352 imp:p=1          $Al casing around detector  35a
353   3 -2.7 -353 354 imp:p=1          $Al casing around detector  35b
355   3 -2.7 -355 356 imp:p=1          $Al casing around detector  35c
361   3 -2.7 -361 362 imp:p=1          $Al casing around detector  36a
363   3 -2.7 -363 364 imp:p=1          $Al casing around detector  36b
365   3 -2.7 -365 366 imp:p=1          $Al casing around detector  36c
371   3 -2.7 -371 372 imp:p=1          $Al casing around detector  37a
373   3 -2.7 -373 374 imp:p=1          $Al casing around detector  37b
375   3 -2.7 -375 376 imp:p=1          $Al casing around detector  37c
381   3 -2.7 -381 382 imp:p=1          $Al casing around detector  38a
383   3 -2.7 -383 384 imp:p=1          $Al casing around detector  38b
385   3 -2.7 -385 386 imp:p=1          $Al casing around detector  38c
441   3 -2.7 -441 442 imp:p=1          $Al casing around detector  44a
443   3 -2.7 -443 444 imp:p=1          $Al casing around detector  44b
445   3 -2.7 -445 446 imp:p=1          $Al casing around detector  44c
411   3 -2.7 -411 412 imp:p=1          $Al casing around detector  41a
413   3 -2.7 -413 414 imp:p=1          $Al casing around detector  41b
415   3 -2.7 -415 416 imp:p=1          $Al casing around detector  41c
421   3 -2.7 -421 422 imp:p=1          $Al casing around detector  42a
423   3 -2.7 -423 424 imp:p=1          $Al casing around detector  42b
425   3 -2.7 -425 426 imp:p=1          $Al casing around detector  42c
431   3 -2.7 -431 432 imp:p=1          $Al casing around detector  43a
433   3 -2.7 -433 434 imp:p=1          $Al casing around detector  43b
435   3 -2.7 -435 436 imp:p=1          $Al casing around detector  43c
451   3 -2.7 -451 452 imp:p=1          $Al casing around detector  45a
453   3 -2.7 -453 454 imp:p=1          $Al casing around detector  45b
455   3 -2.7 -455 456 imp:p=1          $Al casing around detector  45c
461   3 -2.7 -461 462 imp:p=1          $Al casing around detector 46a
463   3 -2.7 -463 464 imp:p=1          $Al casing around detector 46b
465   3 -2.7 -465 466 imp:p=1          $Al casing around detector 46c
471   3 -2.7 -471 472 imp:p=1          $Al casing around detector 47a
473   3 -2.7 -473 474 imp:p=1          $Al casing around detector 47b
475   3 -2.7 -475 476 imp:p=1          $Al casing around detector 47c
481   3 -2.7 -481 482 imp:p=1          $Al casing around detector 48a
483   3 -2.7 -483 484 imp:p=1          $Al casing around detector 48b
485   3 -2.7 -485 486 imp:p=1          $Al casing around detector 44c
140   1 -0.0012048 -140 141 143 145 imp:p=1      $air  around detector 14
110   1 -0.0012048 -110 111 113 115 imp:p=1      $air  around detector 11
120   1 -0.0012048 -120 121 123 125 imp:p=1      $air  around detector 12
130   1 -0.0012048 -130 131 143 145 imp:p=1      $air  around detector 13
150   1 -0.0012048 -150 151 153 155 imp:p=1      $air  around detector 15
160   1 -0.0012048 -160 161 163 165 imp:p=1      $air  around detector 16
170   1 -0.0012048 -170 171 173 175 imp:p=1      $air  around detector 17
180   1 -0.0012048 -180 181 183 185 imp:p=1      $air  around detector 18
240   1 -0.0012048 -240 241 243 245 imp:p=1      $air  around detector 24
210   1 -0.0012048 -210 211 213 215 imp:p=1      $air  around detector 21
220   1 -0.0012048 -220 221 223 225 imp:p=1      $air  around detector 22
```

```
230   1 -0.0012048 -230 231 243 245 imp:p=1      $air  around detector 23
250   1 -0.0012048 -250 251 253 255 imp:p=1      $air  around detector 25
260   1 -0.0012048 -260 261 263 265 imp:p=1      $air  around detector 26
270   1 -0.0012048 -270 271 273 275 imp:p=1      $air  around detector 27
280   1 -0.0012048 -280 281 283 285 imp:p=1      $air  around detector 28
340   1 -0.0012048 -340 341 343 345 imp:p=1      $air  around detector 34
310   1 -0.0012048 -310 311 313 315 imp:p=1      $air  around detector 31
320   1 -0.0012048 -320 321 323 325 imp:p=1      $air  around detector 32
330   1 -0.0012048 -330 331 343 345 imp:p=1      $air  around detector 33
350   1 -0.0012048 -350 351 353 355 imp:p=1      $air  around detector 35
360   1 -0.0012048 -360 361 363 365 imp:p=1      $air  around detector 36
370   1 -0.0012048 -370 371 373 375 imp:p=1      $air  around detector 37
380   1 -0.0012048 -380 381 383 385 imp:p=1      $air  around detector 38
440   1 -0.0012048 -440 441 443 445 imp:p=1      $air  around detector 44
410   1 -0.0012048 -410 411 413 415 imp:p=1      $air  around detector 41
420   1 -0.0012048 -420 421 423 425 imp:p=1      $air  around detector 42
430   1 -0.0012048 -430 431 443 445 imp:p=1      $air  around detector 43
450   1 -0.0012048 -450 451 453 455 imp:p=1      $air  around detector 45
460   1 -0.0012048 -460 461 463 465 imp:p=1      $air  around detector 46
470   1 -0.0012048 -470 471 473 475 imp:p=1      $air  around detector 47
480   1 -0.0012048 -480 481 483 485 imp:p=1      $air  around detector 48
4     1 -0.0012048 -11 #110 #120 #130 #140 #150 #160 #170 #180 &
    #210 #220 #230 #240 #250 #260 #270 #280 #310 #320 #330 #340 #350 #360 &
    #370 #380 #410 #420 #430 #440 #450 #460 #470 #480 imp:p=1    $air space
45    1 -0.0012048 -1 2 -3 12 imp:p=1            $air space to break up cell 4
8     3 -2.7 11 -12 imp:p=1                      $Al aircraft skin
9     4 -2.3 -2 -3 4 imp:p=1                     $source with concrete
10    0 1 imp:p=0                                $void around cylinder
11    0 -4 imp:p=0                               $universe
12    0 -1 3 4 imp:p=0                           $universe

c Surface Card
1    pz 300                                      $plane at 3m above origin
2    pz -20000                                   $ground surface at 200m below detector
3    cz 20000                                    $vertical cylinder with 200m radius
4    pz -20005                                   $bottom of ground surface with 5cm depth
11   rpp -579.8 765.8 -75.2 686.4 -75.2 85.2     $rectangle replicating aircraft
12   rpp -580.1 766.1 -75.5 686.7 -75.5 85.5     $rectangle for aircraft skin
140  rpp -75.2 93 -75.2 115.2 -75.2 85.2         $box around detector 14
141  rpp -0.2 5.2 -0.2 40.2 -0.2 10.2            $2mm thick Al casing for detector 14a
142  rpp 0 5 0 40 0 10                           $NaI detector 5 cm x 40 cm x 10 cm 14a
143  rpp 6.2 11.6 -0.2 40.2 -0.2 10.2            $2mm thick Al casing for detector 14b
144  rpp 6.4 11.4 0 40 0 10                      $NaI detector 5 cm x 40 cm x 10 cm 14b
145  rpp 12.6 18 -0.2 40.2 -0.2 10.2             $2mm thick Al casing for detector 14c
146  rpp 12.8 17.8 0 40 0 10                     $NaI detector 5 cm x 40 cm x 10 cm 14c
110  rpp -579.8 -411.6 -75.2 115.2 -75.2 85.2    $box around detector 11
111  rpp -504.8 -499.4 -0.2 40.2 -0.2 10.2       $2mm thick Al casing detector 11a
112  rpp -504.6 -499.6 0 40 0 10                 $NaI detector 5 cm x 40 cm x 10 cm 11a
113  rpp -498.4 -493 -0.2 40.2 -0.2 10.2         $2mm thick Al casing detector 11b
114  rpp -498.2 -493.2 0 40 0 10                 $NaI detector 5 cm x 40 cm x 10 cm 11b
115  rpp -498.6 -492 -0.2 40.2 -0.2 10.2         $2mm thick Al casing detector 11c
116  rpp -491.8 -486.8 0 40 0 10                 $NaI detector 5 cm x 40 cm x 10 cm 11c
```

```
120  rpp -411.6 -243.4 -75.2 115.2 -75.2 85.2     $box around detector 12
121  rpp -336.6 -331.2 -0.2 40.2 -0.2 10.2        $2mm thick Al casing detector 12a
122  rpp -336.4 -331.4 0 40 0 10                  $NaI detector 5 cm x 40 cm x 10 cm 12a
123  rpp -330.2 -324.8 -0.2 40.2 -0.2 10.2        $2mm thick Al casing detector 12b
124  rpp -330 -325 0 40 0 10                      $NaI detector 5 cm x 40 cm x 10 cm 12b
125  rpp -323.8 -318.4 -0.2 40.2 -0.2 10.2        $2mm thick Al casing detector 12c
126  rpp -323.6 -318.6 0 40 0 10                  $NaI detector 5 cm x 40 cm x 10 cm 12c
130  rpp -243.4 -75.2 -75.2 115.2 -75.2 85.2      $box around detector 13
131  rpp -168.4 -163 -0.2 40.2 -0.2 10.2          $2mm thick Al casing detector 13a
132  rpp -168.2 -163.2 0 40 0 10                  $NaI detector 5 cm x 40 cm x 10 cm 13a
133  rpp -162 -156.6 -0.2 40.2 -0.2 10.2          $2mm thick Al casing detector 13b
134  rpp -161.8 -156.8 0 40 0 10                  $NaI detector 5 cm x 40 cm x 10 cm 13b
135  rpp -155.6 -150.2 -0.2 40.2 -0.2 10.2        $2mm thick Al casing detector 13c
136  rpp -155.4 -150.4 0 40 0 10                  $NaI detector 5 cm x 40 cm x 10 cm 13c
150  rpp 93 261.2 -75.2 115.2 -75.2 85.2          $box around detector 15
151  rpp 168 173.4 -0.2 40.2 -0.2 10.2            $2mm thick Al casing detector 15a
152  rpp 168.2 173.2 0 40 0 10                    $NaI detector 5 cm x 40 cm x 10 cm 15a
153  rpp 174.4 179.8 -0.2 40.2 -0.2 10.2          $2mm thick Al casing detector 15b
154  rpp 174.6 179.6 0 40 0 10                    $NaI detector 5 cm x 40 cm x 10 cm 15b
155  rpp 180.8 186.2 -0.2 40.2 -0.2 10.2          $2mm thick Al casing detector 15c
156  rpp 181 186 0 40 0 10                        $NaI detector 5 cm x 40 cm x 10 cm 15c
160  rpp 261.2 429.4 -75.2 115.2 -75.2 85.2       $box around detector 16
161  rpp 336.2 341.6 -0.2 40.2 -0.2 10.2          $2mm thick Al casing detector 16a
162  rpp 336.4 341.4 0 40 0 10                    $NaI detector 5 cm x 40 cm x 10 cm 16a
163  rpp 342.6 348 -0.2 40.2 -0.2 10.2            $2mm thick Al casing detector 16b
164  rpp 342.8 347.8 0 40 0 10                    $NaI detector 5 cm x 40 cm x 10 cm 16b
165  rpp 349 354.4 -0.2 40.2 -0.2 10.2            $2mm thick Al casing detector 16c
166  rpp 349.2 354.2 0 40 0 10                    $NaI detector 5 cm x 40 cm x 10 cm 16c
170  rpp 429.4 597.6 -75.2 115.2 -75.2 85.2       $box around detector 17
171  rpp 504.4 509.8 -0.2 40.2 -0.2 10.2          $2mm thick Al casing detector 17a
172  rpp 504.6 509.6 0 40 0 10                    $NaI detector 5 cm x 40 cm x 10 cm 17a
173  rpp 510.8 516.2 -0.2 40.2 -0.2 10.2          $2mm thick Al casing detector 17b
174  rpp 511 516 0 40 0 10                        $NaI detector 5 cm x 40 cm x 10 cm 17b
175  rpp 517.2 522.6 -0.2 40.2 -0.2 10.2          $2mm thick Al casing detector 17c
176  rpp 517.4 522.4 0 40 0 10                    $NaI detector 5 cm x 40 cm x 10 cm 17c
180  rpp 597.6 765.8 -75.2 115.2 -75.2 85.2       $box around detector 18
181  rpp 672.6 678 -0.2 40.2 -0.2 10.2            $2mm thick Al casing detector 18a
182  rpp 672.8 677.8 0 40 0 10                    $NaI detector 5 cm x 40 cm x 10 cm 18a
183  rpp 679 684.4 -0.2 40.2 -0.2 10.2            $2mm thick Al casing detector 18b
184  rpp 679.2 684.2 0 40 0 10                    $NaI detector 5 cm x 40 cm x 10 cm 18b
185  rpp 685.4 690.8 -0.2 40.2 -0.2 10.2          $2mm thick Al casing detector 18c
186  rpp 685.6 690.6 0 40 0 10                    $NaI detector 5 cm x 40 cm x 10 cm 18c
240  rpp -75.2 93 115.2 305.6 -75.2 85.2          $box around detector 24
241  rpp -0.2 5.2 190.2 230.6 -0.2 10.2           $2mm thick Al casing detector 24a
242  rpp 0 5 190.4 230.4 0 10                     $NaI detector 5 cm x 40 cm x 10 cm 24a
243  rpp 6.2 11.6 190.2 230.6 -0.2 10.2           $2mm thick Al casing detector 24b
244  rpp 6.4 11.4 190.4 230.4 0 10                $NaI detector 5 cm x 40 cm x 10 cm 24b
245  rpp 12.6 18 190.2 230.6 -0.2 10.2            $2mm thick Al casing detector 24c
246  rpp 12.8 17.8 190.4 230.4 0 10               $NaI detector 5 cm x 40 cm x 10 cm 24c
210  rpp -579.8 -411.6 115.2 305.6 -75.2 85.2     $box around detector 21
211  rpp -504.8 -499.4 190.2 230.6 -0.2 10.2      $2mm thick Al casing detector 21a
212  rpp -504.6 -499.6 190.4 230.4 0 10           $NaI detector 5 cm x 40 cm x 10 cm 21a
```

```
213  rpp -498.4 -493 190.2 230.6 -0.2 10.2        $2mm thick Al casing detector 21b
214  rpp -498.2 -493.2 190.4 230.4 0 10           $NaI detector 5 cm x 40 cm x 10 cm 21b
215  rpp -492 -486.6 190.2 230.6 -0.2 10.2        $2mm thick Al casing detector 21c
216  rpp -491.8 -486.8 190.4 230.4 0 10           $NaI detector 5 cm x 40 cm x 10 cm 21c
220  rpp -411.6 -243.4 115.2 305.6 -75.2 85.2     $box around detector 22
221  rpp -336.6 -331.2 190.2 230.6 -0.2 10.2      $2mm thick Al casing detector 22a
222  rpp -336.4 -331.4 190.4 230.4 0 10           $NaI detector 5 cm x 40 cm x 10 cm 22a
223  rpp -330.2 -324.8 190.2 230.6 -0.2 10.2      $2mm thick Al casing detector 22b
224  rpp -330 -325 190.4 230.4 0 10               $NaI detector 5 cm x 40 cm x 10 cm 22b
225  rpp -323.8 -318.4 190.2 230.6 -0.2 10.2      $2mm thick Al casing detector 22c
226  rpp -323.6 -318.6 190.4 230.4 0 10           $NaI detector 5 cm x 40 cm x 10 cm 22c
230  rpp -243.4 -75.2 115.2 305.6 -75.2 85.2      $box around detector 23
231  rpp -168.4 -163 190.2 230.6 -0.2 10.2        $2mm thick Al casing detector 23a
232  rpp -168.2 -163.2 190.4 230.4 0 10           $NaI detector 5 cm x 40 cm x 10 cm 23a
233  rpp -162 -156.6 190.2 230.6 -0.2 10.2        $2mm thick Al casing detector 23b
234  rpp -161.8 -156.8 190.4 230.4 0 10           $NaI detector 5 cm x 40 cm x 10 cm 23b
235  rpp -155.6 -150.2 190.2 230.6 -0.2 10.2      $2mm thick Al casing detector 23c
236  rpp -155.4 -150.4 190.4 230.4 0 10           $NaI detector 5 cm x 40 cm x 10 cm 23c
250  rpp 93 261.2 115.2 305.6 -75.2 85.2          $box around detector 25
251  rpp 168 173.4 190.2 230.6 -0.2 10.2          $2mm thick Al casing detector 25a
252  rpp 168.2 173.2 190.4 230.4 0 10             $NaI detector 5 cm x 40 cm x 10 cm 25a
253  rpp 174.4 179.8 190.2 230.6 -0.2 10.2        $2mm thick Al casing detector 25b
254  rpp 174.6 179.6 190.4 230.4 0 10             $NaI detector 5 cm x 40 cm x 10 cm 25b
255  rpp 180.8 186.2 190.2 230.6 -0.2 10.2        $2mm thick Al casing detector 25c
256  rpp 181 186 190.4 230.4 0 10                 $NaI detector 5 cm x 40 cm x 10 cm 25c
260  rpp 261.2 429.4 115.2 305.6 -75.2 85.2       $box around detector 26
261  rpp 336.2 341.6 190.2 230.6 -0.2 10.2        $2mm thick Al casing detector 26a
262  rpp 336.4 341.4 190.4 230.4 0 10             $NaI detector 5 cm x 40 cm x 10 cm 26a
263  rpp 342.6 348 190.2 230.6 -0.2 10.2          $2mm thick Al casing detector 26b
264  rpp 342.8 347.8 190.4 230.4 0 10             $NaI detector 5 cm x 40 cm x 10 cm 26b
265  rpp 349 354.4 190.2 230.6 -0.2 10.2          $2mm thick Al casing detector 26c
266  rpp 349.2 354.2 190.4 230.4 0 10             $NaI detector 5 cm x 40 cm x 10 cm 26c
270  rpp 429.4 597.6 115.2 305.6 -75.2 85.2       $box around detector 27
271  rpp 504.4 509.8 190.2 230.6 -0.2 10.2        $2mm thick Al casing detector 27a
272  rpp 504.6 509.6 190.4 230.4 0 10             $NaI detector 5 cm x 40 cm x 10 cm 27a
273  rpp 510.8 516.2 190.2 230.6 -0.2 10.2        $2mm thick Al casing detector 27b
274  rpp 511 516 190.4 230.4 0 10                 $NaI detector 5 cm x 40 cm x 10 cm 27b
275  rpp 517.2 522.6 190.2 230.6 -0.2 10.2        $2mm thick Al casing detector 27c
276  rpp 517.4 522.4 190.4 230.4 0 10             $NaI detector 5 cm x 40 cm x 10 cm 27c
280  rpp 597.6 765.8 115.2 305.6 -75.2 85.2       $box around detector 28
281  rpp 672.6 678 190.2 230.6 -0.2 10.2          $2mm thick Al casing detector 28a
282  rpp 672.8 677.8 190.4 230.4 0 10             $NaI detector 5 cm x 40 cm x 10 cm 28a
283  rpp 679 684.4 190.2 230.6 -0.2 10.2          $2mm thick Al casing detector 28b
284  rpp 679.2 684.2 190.4 230.4 0 10             $NaI detector 5 cm x 40 cm x 10 cm 28b
285  rpp 685.4 690.8 190.2 230.6 -0.2 10.2        $2mm thick Al casing detector 28c
286  rpp 685.6 690.6 190.4 230.4 0 10             $NaI detector 5 cm x 40 cm x 10 cm 28c
340  rpp -75.2 93 305.6 496 -75.2 85.2            $box around detector 34
341  rpp -0.2 5.2 380.6 421 -0.2 10.2             $2mm thick Al casing detector 34a
342  rpp 0 5 380.8 420.8 0 10                     $NaI detector 5 cm x 40 cm x 10 cm 34a
343  rpp 6.2 11.6 380.6 421 -0.2 10.2             $2mm thick Al casing detector 34b
344  rpp 6.4 11.4 380.8 420.8 0 10                $NaI detector 5 cm x 40 cm x 10 cm 34b
345  rpp 12.6 18 380.6 421 -0.2 10.2              $2mm thick Al casing detector 34c
```

```
346  rpp 12.8 17.8 380.8 420.8 0 10          $NaI detector 5 cm x 40 cm x 10 cm 34c
310  rpp -579.8 -411.6 305.6 496 -75.2 85.2  $box around detector 31
311  rpp -504.8 -499.4 380.6 421 -0.2 10.2   $2mm thick Al casing detector 31a
312  rpp -504.6 -499.6 380.8 420.8 0 10      $NaI detector 5 cm x 40 cm x 10 cm 31a
313  rpp -498.4 -493 380.6 421 -0.2 10.2     $2mm thick Al casing detector 31b
314  rpp -498.2 -493.2 380.8 420.8 0 10      $NaI detector 5 cm x 40 cm x 10 cm 31b
315  rpp -492 -486.6 380.6 421 -0.2 10.2     $2mm thick Al casing detector 31c
316  rpp -491.8 -486.8 380.8 420.8 0 10      $NaI detector 5 cm x 40 cm x 10 cm 31c
320  rpp -411.6 -243.4 305.6 496 -75.2 85.2  $box around detector 32
321  rpp -336.6 -331.2 380.6 421 -0.2 10.2   $2mm thick Al casing detector 32a
322  rpp -336.4 -331.4 380.8 420.8 0 10      $NaI detector 5 cm x 40 cm x 10 cm 32a
323  rpp -330.2 -324.8 380.6 421 -0.2 10.2   $2mm thick Al casing detector 32b
324  rpp -330 -325 380.8 420.8 0 10          $NaI detector 5 cm x 40 cm x 10 cm 32b
325  rpp -323.8 -318.4 380.6 421 -0.2 10.2   $2mm thick Al casing detector 32c
326  rpp -323.6 -318.6 380.8 420.8 0 10      $NaI detector 5 cm x 40 cm x 10 cm 32c
330  rpp -243.4 -75.2 305.6 496 -75.2 85.2   $box around detector 33
331  rpp -168.4 -163 380.6 421 -0.2 10.2     $2mm thick Al casing detector 33a
332  rpp -168.2 -163.2 380.8 420.8 0 10      $NaI detector 5 cm x 40 cm x 10 cm 33a
333  rpp -162 -156.6 380.6 421 -0.2 10.2     $2mm thick Al casing detector 33b
334  rpp -161.8 -156.8 380.8 420.8 0 10      $NaI detector 5 cm x 40 cm x 10 cm 33b
335  rpp -155.6 -150.2 380.6 421 -0.2 10.2   $2mm thick Al casing detector 33c
336  rpp -155.4 -150.4 380.8 420.8 0 10      $NaI detector 5 cm x 40 cm x 10 cm 33c
350  rpp 93 261.2 305.6 496 -75.2 85.2       $box around detector 35
351  rpp 168 173.4 380.6 421 -0.2 10.2       $2mm thick Al casing detector 35a
352  rpp 168.2 173.2 380.8 420.8 0 10        $NaI detector 5 cm x 40 cm x 10 cm 35a
353  rpp 174.4 179.8 380.6 421 -0.2 10.2     $2mm thick Al casing detector 35b
354  rpp 174.6 179.6 380.8 420.8 0 10        $NaI detector 5 cm x 40 cm x 10 cm 35b
355  rpp 180.8 186.2 380.6 421 -0.2 10.2     $2mm thick Al casing detector 35c
356  rpp 181 186 380.8 420.8 0 10            $NaI detector 5 cm x 40 cm x 10 cm 35c
360  rpp 261.2 429.4 305.6 496 -75.2 85.2    $box around detector 36
361  rpp 336.2 341.6 380.6 421 -0.2 10.2     $2mm thick Al casing detector 36a
362  rpp 336.4 341.4 380.8 420.8 0 10        $NaI detector 5 cm x 40 cm x 10 cm 36a
363  rpp 342.6 348 380.6 421 -0.2 10.2       $2mm thick Al casing detector 36b
364  rpp 342.8 347.8 380.8 420.8 0 10        $NaI detector 5 cm x 40 cm x 10 cm 36b
365  rpp 349 354.4 380.6 421 -0.2 10.2       $2mm thick Al casing detector 36c
366  rpp 349.2 354.2 380.8 420.8 0 10        $NaI detector 5 cm x 40 cm x 10 cm 36c
370  rpp 429.4 597.6 305.6 496 -75.2 85.2    $box around detector 37
371  rpp 504.4 509.8 380.6 421 -0.2 10.2     $2mm thick Al casing detector 37a
372  rpp 504.6 509.6 380.8 420.8 0 10        $NaI detector 5 cm x 40 cm x 10 cm 37a
373  rpp 510.8 516.2 380.6 421 -0.2 10.2     $2mm thick Al casing detector 37b
374  rpp 511 516 380.8 420.8 0 10            $NaI detector 5 cm x 40 cm x 10 cm 37b
375  rpp 517.2 522.6 380.6 421 -0.2 10.2     $2mm thick Al casing detector 37c
376  rpp 517.4 522.4 380.8 420.8 0 10        $NaI detector 5 cm x 40 cm x 10 cm 37c
380  rpp 597.6 765.8 305.6 496 -75.2 85.2    $box around detector 38
381  rpp 672.6 678 380.6 421 -0.2 10.2       $2mm thick Al casing detector 38a
382  rpp 672.8 677.8 380.8 420.8 0 10        $NaI detector 5 cm x 40 cm x 10 cm 38a
383  rpp 679 684.4 380.6 421 -0.2 10.2       $2mm thick Al casing detector 38b
384  rpp 679.2 684.2 380.8 420.8 0 10        $NaI detector 5 cm x 40 cm x 10 cm 38b
385  rpp 685.4 690.8 380.6 421 -0.2 10.2     $2mm thick Al casing detector 38c
386  rpp 685.6 690.6 380.8 420.8 0 10        $NaI detector 5 cm x 40 cm x 10 cm 38c
440  rpp -75.2 93 496 686.4 -75.2 85.2       $box around detector 44
441  rpp -0.2 5.2 571 611.4 -0.2 10.2        $2mm thick Al casing detector 44a
```

```
442  rpp 0 5 571.2 611.2 0 10                $NaI detector 5 cm x 40 cm x 10 cm 44a
443  rpp 6.2 11.6 571 611.4 -0.2 10.2        $2mm thick Al casing detector 44b
444  rpp 6.4 11.4 571.2 611.2 0 10           $NaI detector 5 cm x 40 cm x 10 cm 44b
445  rpp 12.6 18 571 611.4 -0.2 10.2         $2mm thick Al casing detector 44c
446  rpp 12.8 17.8 571.2 611.2 0 10          $NaI detector 5 cm x 40 cm x 10 cm 44c
410  rpp -579.8 -411.6 496 686.4 -75.2 85.2  $box around detector 41
411  rpp -504.8 -499.4 571 611.4 -0.2 10.2   $2mm thick Al casing detector 41a
412  rpp -504.6 -499.6 571.2 611.2 0 10      $NaI detector 5 cm x 40 cm x 10 cm 41a
413  rpp -498.4 -493 571 611.4 -0.2 10.2     $2mm thick Al casing detector 41b
414  rpp -498.2 -493.2 571.2 611.2 0 10      $NaI detector 5 cm x 40 cm x 10 cm 41b
415  rpp -492 -486.6 571 611.4 -0.2 10.2     $2mm thick Al casing detector 41c
416  rpp -491.8 -486.8 571.2 611.2 0 10      $NaI detector 5 cm x 40 cm x 10 cm 41c
420  rpp -411.6 -243.4 496 686.4 -75.2 85.2  $box around detector 42
421  rpp -336.6 -331.2 571 611.4 -0.2 10.2   $2mm thick Al casing detector 42a
422  rpp -336.4 -331.4 571.2 611.2 0 10      $NaI detector 5 cm x 40 cm x 10 cm 42a
423  rpp -330.2 -324.8 571 611.4 -0.2 10.2   $2mm thick Al casing detector 42b
424  rpp -330 -325 571.2 611.2 0 10          $NaI detector 5 cm x 40 cm x 10 cm 42b
425  rpp -323.8 -318.4 571 611.4 -0.2 10.2   $2mm thick Al casing detector 42c
426  rpp -323.6 -318.6 571.2 611.2 0 10      $NaI detector 5 cm x 40 cm x 10 cm 42c
430  rpp -243.4 -75.2 496 686.4 -75.2 85.2   $box around detector 43
431  rpp -168.4 -163 571 611.4 -0.2 10.2     $2mm thick Al casing detector 43a
432  rpp -168.2 -163.2 571.2 611.2 0 10      $NaI detector 5 cm x 40 cm x 10 cm 43a
433  rpp -162 -156.6 571 611.4 -0.2 10.2     $2mm thick Al casing detector 43b
434  rpp -161.8 -156.8 571.2 611.2 0 10      $NaI detector 5 cm x 40 cm x 10 cm 43b
435  rpp -155.6 -150.2 571 611.4 -0.2 10.2   $2mm thick Al casing detector 43c
436  rpp -155.4 -150.4 571.2 611.2 0 10      $NaI detector 5 cm x 40 cm x 10 cm 43c
450  rpp 93 261.2 496 686.4 -75.2 85.2       $box around detector 45
451  rpp 168 173.4 571 611.4 -0.2 10.2       $2mm thick Al casing detector 45a
452  rpp 168.2 173.2 571.2 611.2 0 10        $NaI detector 5 cm x 40 cm x 10 cm 45a
453  rpp 174.4 179.8 571 611.4 -0.2 10.2     $2mm thick Al casing detector 45b
454  rpp 174.6 179.6 571.2 611.2 0 10        $NaI detector 5 cm x 40 cm x 10 cm 45b
455  rpp 180.8 186.2 571 611.4 -0.2 10.2     $2mm thick Al casing detector 45c
456  rpp 181 186 571.2 611.2 0 10            $NaI detector 5 cm x 40 cm x 10 cm 45c
460  rpp 261.2 429.4 496 686.4 -75.2 85.2    $box around detector 46
461  rpp 336.2 341.6 571 611.4 -0.2 10.2     $2mm thick Al casing detector 46a
462  rpp 336.4 341.4 571.2 611.2 0 10        $NaI detector 5 cm x 40 cm x 10 cm 46a
463  rpp 342.6 348 571 611.4 -0.2 10.2       $2mm thick Al casing detector 46b
464  rpp 342.8 347.8 571.2 611.2 0 10        $NaI detector 5 cm x 40 cm x 10 cm 46b
465  rpp 349 354.4 571 611.4 -0.2 10.2       $2mm thick Al casing detector 46c
466  rpp 349.2 354.2 571.2 611.2 0 10        $NaI detector 5 cm x 40 cm x 10 cm 46c
470  rpp 429.4 597.6 496 686.4 -75.2 85.2    $box around detector 47
471  rpp 504.4 509.8 571 611.4 -0.2 10.2     $2mm thick Al casing detector 47a
472  rpp 504.6 509.6 571.2 611.2 0 10        $NaI detector 5 cm x 40 cm x 10 cm 47a
473  rpp 510.8 516.2 571 611.4 -0.2 10.2     $2mm thick Al casing detector 47b
474  rpp 511 516 571.2 611.2 0 10            $NaI detector 5 cm x 40 cm x 10 cm 47b
475  rpp 517.2 522.6 571 611.4 -0.2 10.2     $2mm thick Al casing detector 47c
476  rpp 517.4 522.4 571.2 611.2 0 10        $NaI detector 5 cm x 40 cm x 10 cm 47c
480  rpp 597.6 765.8 496 686.4 -75.2 85.2    $box around detector 48
481  rpp 672.6 678 571 611.4 -0.2 10.2       $2mm thick Al casing detector 48a
482  rpp 672.8 677.8 571.2 611.2 0 10        $NaI detector 5 cm x 40 cm x 10 cm 48a
483  rpp 679 684.4 571 611.4 -0.2 10.2       $2mm thick Al casing detector 48b
484  rpp 679.2 684.2 571.2 611.2 0 10        $NaI detector 5 cm x 40 cm x 10 cm 48b
```

```
485  rpp 685.4 690.8 571 611.4 -0.2 10.2          $2mm thick Al casing detector 48c
486  rpp 685.6 690.6 571.2 611.2 0 10             $NaI detector 5 cm x 40 cm x 10 cm 48c

c Data Cards
c Source Homogeneous Distribution of nuclide in air for 200m
sdef sur=4 pos=0 0 -20000 rad=d1 erg=0.662 par=2      $source definition for Cs-137
c sdef sur=4 pos=0 0 -20000 rad=d1 erg=d2 par=2       $source definition for Cs-134
c sdef sur=4 pos=0 0 -20000 rad=d1 erg=d2 par=2       $source definition for I-131
si1 h 0 19999                                         $spherical source located outside aircraft
sp1 -21 1
c si2 l 0.605 0.796                                   $Cs-134 energies
c sp2 0.6853 0.2333
c si2 l 0.284 0.364 0.637                             $I-131 energies
c sp2 0.0548 0.730 0.00487
mode p                                                $photons
nps  1000000000                                       $1 billion particles
m1   007014 -0.7553                                   $air density = 0.0012048 g/cm^3
     008016 -0.2318
     018000 -0.01282
     006012 -0.000125
m2   011000 -0.5                                      $NaI density 3.67 g/cm^3
     053000 -0.5
m3   013000 -1                                        $Al density 2.7 g/cm^3
m4   001000 0.1170                                    $concrete "standard" 2.3 g/cm^3
     008016 0.6082
     014000 0.2748
c F8 Tally energy deposition
F18:p 142            $detector 14a
#   E18
   0
   0.010
   0.500
   0.700
   10
F28:p 144            $detector 14b
#   E28
   0
   0.010
   0.500
   0.700
   10
F38:p 146            $detector 14c
#   E38
   0
   0.010
   0.500
   0.700
   10
F48:p 112            $detector 11a
#   E48
   0
   0.010
```

```
   0.500
   0.700
   10
F58:p 114          $detector 11b
#   E58
   0
   0.010
   0.500
   0.700
   10
F68:p 116          $detector 11c
#   E68
   0
   0.010
   0.500
   0.700
   10
F78:p 122          $detector 12a
#   E78
   0
   0.010
   0.500
   0.700
   10
F88:p 124          $detector 12b
#   E88
   0
   0.010
   0.500
   0.700
   10
F98:p 126          $detector 12c
#   E98
   0
   0.010
   0.500
   0.700
   10
F108:p 132          $detector 13a
#   E108
   0
   0.010
   0.500
   0.700
   10
F118:p 134          $detector 13b
#   E118
   0
   0.010
   0.500
   0.700
   10
```

```
F128:p 136          $detector 13c
#   E128
   0
   0.010
   0.500
   0.700
   10
F138:p 152          $detector 15a
#   E138
   0
   0.010
   0.500
   0.700
   10
F148:p 154          $detector 15b
#   E148
   0
   0.010
   0.500
   0.700
   10
F158:p 156          $detector 15c
#   E158
   0
   0.010
   0.500
   0.700
   10
F168:p 162          $detector 16a
#   E168
   0
   0.010
   0.500
   0.700
   10
F178:p 164          $detector 16b
#   E178
   0
   0.010
   0.500
   0.700
   10
F188:p 166          $detector 16c
#   E188
   0
   0.010
   0.500
   0.700
   10
F198:p 172          $detector 17a
#   E198
   0
```

```
   0.010
   0.500
   0.700
   10
F208:p 174          $detector 17b
#   E208
   0
   0.010
   0.500
   0.700
   10
F218:p 176          $detector 17c
#   E218
   0
   0.010
   0.500
   0.700
   10
F228:p 182          $detector 18a
#   E228
   0
   0.010
   0.500
   0.700
   10
F238:p 184          $detector 18b
#   E238
   0
   0.010
   0.500
   0.700
   10
F248:p 186          $detector 18c
#   E248
   0
   0.010
   0.500
   0.700
   10
F258:p 242          $detector 24a
#   E258
   0
   0.010
   0.500
   0.700
   10
F268:p 244          $detector 24b
#   E268
   0
   0.010
   0.500
   0.700
```

```
   10
F278:p 246          $detector 24c
#   E278
   0
   0.010
   0.500
   0.700
   10
F288:p 212          $detector 21a
#   E288
   0
   0.010
   0.500
   0.700
   10
F298:p 214          $detector 21b
#   E298
   0
   0.010
   0.500
   0.700
   10
F308:p 216          $detector 21c
#   E308
   0
   0.010
   0.500
   0.700
   10
F318:p 222          $detector 22a
#   E318
   0
   0.010
   0.500
   0.700
   10
F328:p 224          $detector 22b
#   E328
   0
   0.010
   0.500
   0.700
   10
F338:p 226          $detector 22c
#   E338
   0
   0.010
   0.500
   0.700
   10
F348:p 232          $detector 23a
#   E348
```

```
   0
   0.010
   0.500
   0.700
   10
F358:p 234          $detector 23b
#   E358
   0
   0.010
   0.500
   0.700
   10
F368:p 236          $detector 23c
#   E368
   0
   0.010
   0.500
   0.700
   10
F378:p 252          $detector 25a
#   E378
   0
   0.010
   0.500
   0.700
   10
F388:p 254          $detector 25b
#   E388
   0
   0.010
   0.500
   0.700
   10
F398:p 256          $detector 25c
#   E398
   0
   0.010
   0.500
   0.700
   10
F408:p 262          $detector 26a
#   E408
   0
   0.010
   0.500
   0.700
   10
F418:p 264          $detector 26b
#   E418
   0
   0.010
   0.500
```

```
   0.700
   10
F428:p 266          $detector 26c
#   E428
   0
   0.010
   0.500
   0.700
   10
F438:p 272          $detector 27a
#   E438
   0
   0.010
   0.500
   0.700
   10
F448:p 274          $detector 27b
#   E448
   0
   0.010
   0.500
   0.700
   10
F458:p 276          $detector 27c
#   E458
   0
   0.010
   0.500
   0.700
   10
F468:p 282          $detector 28a
#   E468
   0
   0.010
   0.500
   0.700
   10
F478:p 284          $detector 28b
#   E478
   0
   0.010
   0.500
   0.700
   10
F488:p 286          $detector 28c
#   E488
   0
   0.010
   0.500
   0.700
   10
F498:p 342          $detector 34a
```

```
#   E498
   0
   0.010
   0.500
   0.700
   10
F508:p 344          $detector 34b
#   E508
   0
   0.010
   0.500
   0.700
   10
F518:p 346          $detector 34c
#   E518
   0
   0.010
   0.500
   0.700
   10
F528:p 312          $detector 31a
#   E528
   0
   0.010
   0.500
   0.700
   10
F538:p 314          $detector 31b
#   E538
   0
   0.010
   0.500
   0.700
   10
F548:p 316          $detector 31c
#   E548
   0
   0.010
   0.500
   0.700
   10
F558:p 322          $detector 32a
#   E558
   0
   0.010
   0.500
   0.700
   10
F568:p 324          $detector 32b
#   E568
   0
   0.010
```

```
   0.500
   0.700
   10
F578:p 326          $detector 32c
#   E578
   0
   0.010
   0.500
   0.700
   10
F588:p 332          $detector 33a
#   E588
   0
   0.010
   0.500
   0.700
   10
F598:p 334          $detector 33b
#   E598
   0
   0.010
   0.500
   0.700
   10
F608:p 336          $detector 33c
#   E608
   0
   0.010
   0.500
   0.700
   10
F618:p 352          $detector 35a
#   E618
   0
   0.010
   0.500
   0.700
   10
F628:p 354          $detector 35b
#   E628
   0
   0.010
   0.500
   0.700
   10
F638:p 356          $detector 35c
#   E638
   0
   0.010
   0.500
   0.700
   10
```

```
F648:p 362          $detector 36a
#   E648
   0
   0.010
   0.500
   0.700
   10
F658:p 364          $detector 36b
#   E658
   0
   0.010
   0.500
   0.700
   10
F668:p 366          $detector 36c
#   E668
   0
   0.010
   0.500
   0.700
   10
F678:p 372          $detector 37a
#   E678
   0
   0.010
   0.500
   0.700
   10
F688:p 374          $detector 37b
#   E688
   0
   0.010
   0.500
   0.700
   10
F698:p 376          $detector 37c
#   E698
   0
   0.010
   0.500
   0.700
   10
F708:p 382          $detector 38a
#   E708
   0
   0.010
   0.500
   0.700
   10
F718:p 384          $detector 38b
#   E718
   0
```

```
   0.010
   0.500
   0.700
   10
F728:p 386          $detector 38c
#   E728
   0
   0.010
   0.500
   0.700
   10
F738:p 442          $detector 44a
#   E738
   0
   0.010
   0.500
   0.700
   10
F748:p 444          $detector 44b
#   E748
   0
   0.010
   0.500
   0.700
   10
F758:p 446          $detector 44c
#   E758
   0
   0.010
   0.500
   0.700
   10
F768:p 412          $detector 41a
#   E768
   0
   0.010
   0.500
   0.700
   10
F778:p 414          $detector 41b
#   E778
   0
   0.010
   0.500
   0.700
   10
F788:p 416          $detector 41c
#   E788
   0
   0.010
   0.500
   0.700
```

```
   10
F798:p 422          $detector 42a
#   E798
   0
   0.010
   0.500
   0.700
   10
F808:p 424          $detector 42b
#   E808
   0
   0.010
   0.500
   0.700
   10
F818:p 426          $detector 42c
#   E818
   0
   0.010
   0.500
   0.700
   10
F828:p 432          $detector 43a
#   E828
   0
   0.010
   0.500
   0.700
   10
F838:p 434          $detector 43b
#   E838
   0
   0.010
   0.500
   0.700
   10
F848:p 436          $detector 43c
#   E848
   0
   0.010
   0.500
   0.700
   10
F858:p 452          $detector 45a
#   E858
   0
   0.010
   0.500
   0.700
   10
F868:p 454          $detector 45b
#   E868
```

```
   0
   0.010
   0.500
   0.700
   10
F878:p 456          $detector 45c
#   E878
   0
   0.010
   0.500
   0.700
   10
F888:p 462          $detector 46a
#   E888
   0
   0.010
   0.500
   0.700
   10
F898:p 464          $detector 46b
#   E898
   0
   0.010
   0.500
   0.700
   10
F908:p 466          $detector 46c
#   E908
   0
   0.010
   0.500
   0.700
   10
F918:p 472          $detector 47a
#   E918
   0
   0.010
   0.500
   0.700
   10
F928:p 474          $detector 47b
#   E928
   0
   0.010
   0.500
   0.700
   10
F938:p 476          $detector 47c
#   E938
   0
   0.010
   0.500
```

```
   0.700
   10
F948:p 482          $detector 48a
#   E948
   0
   0.010
   0.500
   0.700
   10
F958:p 484          $detector 48b
#   E958
   0
   0.010
   0.500
   0.700
   10
F968:p 486          $detector 48c
#   E968
   0
   0.010
   0.500
   0.700
   10
```

APPENDIX D: GROUND VS. AERIAL ACTIVITY CONCENTRATIONS

The measured activity concentrations in units of Bq/m^3 from the ground air samples were compared to the expected activity concentration, also given in units of Bq/m^3. Comparison of decay-corrected ground air samples with representative results for the stated nuclides, exclusive of those depicted in Table 5, compared to calculated activity concentrations of net aerial gamma count rates is depicted in Table 8. Note that the dashed lines in the table represent non-detectable results and that the calculated averages omit this number from consideration.

Table 8: Comparison of decay-corrected ground air samples without representative results for all three nuclides of interest (^{134}Cs, ^{137}Cs, and ^{131}I), compared to calculated activity concentrations of net aerial gamma count rates. Note that the dashed lines in the table represent non-detectable results and that the calculated averages omit this number from consideration.

Ground Sample ID	Nuclide(s) Represented in Ground Sample	Decay-corrected Measured Ground Air Activity Concentration (Bq/m^3)	Calculated Aerial Activity Concentration (Bq/m^3)	Comparison of Ground vs. Aerial Activity Concentrations
SCF-00068	^{137}Cs and ^{131}I	3.107	5825.018	0.053%
SCF-00095	^{137}Cs and ^{131}I	175.234	77026.179	0.227%
SCF-00143	^{137}Cs and ^{131}I	15.154	51377.109	0.029%
SCF-07627	^{137}Cs and ^{131}I	0.295	28255.276	0.001%
SCF-07635	^{137}Cs and ^{131}I	1.234	28255.276	0.004%
SCF-00001	^{131}I only	1.043	11321.365	0.009%
SCF-00029	^{131}I only	0.615	61514.277	0.001%
SCF-00049	^{131}I only	0.248	31946.491	0.001%
SCF-00060	^{131}I only	1.688	1390.202	0.121%
SCF-00062	^{131}I only	1.698	297.234	0.571%
SCF-00066	^{131}I only	1.886	-	-
SCF-00067	^{131}I only	2.990	5827.369	0.051%
SCF-00071	^{131}I only	1.744	13074.440	0.013%
SCF-00072	^{131}I only	1.743	13074.440	0.013%
SCF-00097	^{131}I only	63.354	40207.448	0.158%
SCF-00206	^{131}I only	0.211	297.234	0.071%
SCF-00207	^{131}I only	0.425	297.234	0.143%
SCF-07628	^{131}I only	0.238	11321.365	0.002%
SCF-07668	^{131}I only	0.204	61514.277	0.000%
SCF-07670	^{131}I only	1.685	61514.277	0.003%
SCF-08221	^{131}I only	0.166	40030.728	0.000%
SCF-08644	^{131}I only	0.070	3061.025	0.002%
SCF-08802	^{137}Cs only	0.070	10873.302	0.001%
Average:		11.961	25377.344	0.067%

APPENDIX E: ESTIMATED GROUND DEPOSITION

Estimated ground deposition calculated from measured aerial net gamma count rate minus the expected net count rate based upon the measured ground air samples, adjusted to ground level, inclusive of the ground air samples with representative results for ^{134}Cs, ^{137}Cs, and ^{131}I, exclusive of those depicted in Table 6 is depicted in Table 9. Note that the dashed lines in the table represent non-detectable results and that the calculated averages omit this number from consideration.

Table 9: Estimated ground deposition calculated from measured aerial net gamma count rate minus the expected net count rate based upon the measured ground air samples, inclusive of the ground air samples without representative results for all three nuclides of interest (^{134}Cs, ^{137}Cs, and ^{131}I). Note that the dashed lines in the table represent non-detectable results and the calculated averages omit this number from consideration.

Ground Sample ID	Nuclide(s) Represented in Ground Sample	Expected Net Count Rate Based on Ground Air Sample (sec^{-1})	Actual Net Count Rate Minus Expected Net Count Rate (sec^{-1})	Net Counts Divided by Area Covered by Aircraft (cps/m^2)	Estimated Ground deposition (Bq/m^2)
SCF-00068	^{137}Cs and ^{131}I	3.797	7113.846	3.069E-03	3.754E+07
SCF-00095	^{137}Cs and ^{131}I	214.038	93904.950	2.534E-01	6.839E+05
SCF-00143	^{137}Cs and ^{131}I	18.511	62759.644	2.534E-01	8.588E+06
SCF-07627	^{137}Cs and ^{131}I	0.362	34525.016	1.022E-01	9.064E+05
SCF-07635	^{137}Cs and ^{131}I	1.510	34523.869	1.022E-01	9.064E+05
SCF-00001	^{131}I only	1.274	13826.826	4.669E-04	8.055E+08
SCF-00029	^{131}I only	0.751	75133.787	1.307E-01	8.681E+05
SCF-00049	^{131}I only	0.303	39019.661	2.538E-01	2.677E+05
SCF-00060	^{131}I only	2.061	1695.955	7.889E-04	2.532E+07
SCF-00062	^{131}I only	2.073	360.973	3.012E+02	3.035E+06
SCF-00066	^{131}I only	2.304	-	-	-
SCF-00067	^{131}I only	3.652	7113.991	3.070E-03	3.789E+07
SCF-00071	^{131}I only	2.131	15967.203	1.266E-02	1.130E+07
SCF-00072	^{131}I only	2.129	15967.205	1.266E-02	1.130E+07
SCF-00097	^{131}I only	77.382	49032.648	2.292E-01	4.125E+05
SCF-00206	^{131}I only	0.258	362.788	3.086E-04	3.050E+06
SCF-00207	^{131}I only	0.519	362.527	3.084E-04	3.048E+06
SCF-07628	^{131}I only	0.290	13827.809	4.670E-04	8.056E+08
SCF-07668	^{131}I only	0.249	75134.290	1.307E-01	8.681E+05
SCF-07670	^{131}I only	2.058	75132.480	1.307E-01	8.681E+05
SCF-08221	^{131}I only	0.203	48893.980	2.239E-01	4.707E+05
SCF-08644	^{131}I only	0.085	3738.701	1.780E-03	2.871E+07
SCF-08802	^{137}Cs only	0.087	13844.702	4.674E-04	1.868E+07
Average:		14.61	31011.039	13.775	8.21E+07